SIAM J. Applied Dynamical Systems
Vol. 15, No. 2, pp. 1193–1226
© 2016 Society for Industrial and Applied Mathematics

Coarse-Graining and Simplification of the Dynamics Seen in Bursting Neurons*

A. Ben-Tal† and I. G. Kevrekidis‡

Abstract. A system of coupled bursting neurons often exhibits transitions from a quiescent state (no action potentials) to a bursting state (where there are several action potentials in each burst and periods of no action potentials between bursts) to a spiking state (continuous train of action potentials). However, in certain applications, the exact details of the complex dynamics that underlies these transitions may not be important and one would like to use a simplified model that captures the dynamics only roughly. We have developed a numerical method, based on an equation-free approach, that enables us to rationalize the type of bifurcations the simplified model ought to exhibit. The method maps between the variables of a bursting neural network (for which the equations are known) and the variables of a simplified model (for which the equations are in principle unknown). By moving back and forth between the variables of the detailed system and the variables of the simplified system using restriction and lifting operators, and simulating the detailed system for short periods of time, we can calculate the stationary solutions of the simplified model and their effective stabilities and create bifurcation diagrams for the simplified model. We illustrate our approach on a model of a single neuron that consists of three ordinary differential equations and show that the system could be simplified using two ordinary differential equations. We then show how our method can be applied to a network of several neurons. Our work is motivated by studies of the neural control of breathing.

Key words. model reduction, equation-free, bifurcation, pre-Bötzinger complex

AMS subject classification. 37Mxx

DOI. 10.1137/151004574

1. Introduction.

Every model is an approximation of reality and as such could sometimes be fit for purpose and sometimes not. Deciding whether a model could serve its purpose involves some degree of subjectivity. Arguably, models at different levels of description are needed for different purposes (analogous to geographic maps at different scales or different level of detail), but what is the right level of description for a particular purpose? To explore this modelling question we study a particular example concerning the pre-Bötzinger complex (pre-BötC).

The pre-BötC is an area of the mammalian brainstem that is essential for producing the neural breathing rhythm [12, 24, 37]. It has been studied extensively both experimentally (see, for example, [12, 38]) and computationally (see, for example, [7, 8, 14, 24, 42]) and has been shown to exhibit complex dynamic behavior. Neurons in the pre-BötC can generate a

*Received by the editors January 20, 2015; accepted for publication (in revised form) by J. Rubin April 7, 2016; published electronically June 21, 2016.

http://www.siam.org/journals/siads/15-2/100457.html

†Institute of Natural and Mathematical Sciences, Massey University, Albany Campus, 0745, Auckland, New Zealand (a.ben-tal@massey.ac.nz). This author's research was partially supported by the Marsden Fund Council from Government funding, administered by the Royal Society of New Zealand.

‡Department of Chemical and Biological Engineering and PACM, Princeton University, Princeton, NJ 08544 (yannis@arnold.princeton.edu). This author's work was partially supported by the U.S. National Science Foundation and the U.S. Air Force Office of Scientific Research (Dr. F. Darema).

Downloaded 12/19/19 to 128.112.173.161. Redistribution subject to SIAM license or copyright; see http://www.siam.org/journals/ojsa.php

Copyright © by SIAM. Unauthorized reproduction of this article is prohibited.

Downloaded 12/19/19 to 128.112.173.161. Redistribution subject to SIAM license or copyright; see http://www.siam.org/journals/ojsa.php

pattern of bursting (where there are several action potentials in each burst and periods of no action potentials between bursts) at different bursting frequencies and could also operate in a quiescent state (where there are no action potentials) or a spiking state (where there is a continuous train of action potentials). Both the spiking state and the bursting state could themselves be chaotic for a range of parameter values, and as the number of spikes per burst increases, the dynamic response may also involve chaotic behavior over a small range of parameter values [11, 39, 40]. While these complexities may be relevant at the level of the pre-BötC (and are exciting from a dynamical systems point of view), they may not be so important when the pre-BötC is embedded in, and interacts with, other systems. For example, in the integrated respiratory system, the train of action potentials generated by the pre-BötC activates the respiratory muscle (diaphragm) downstream (via other populations of neurons), causing it to contract and leading to movement of air into the lungs (during the quiescent period, the diaphragm relaxes and air moves out of the lungs) [24]. Provided the spikes are dense enough, the diaphragm will contract whether the spiking is chaotic or not, effectively filtering out the neural signal. This physiological reality motivates the simplification of models of the pre-BötC, as it provides a major advantage in studies of the integrated behavior of the respiratory system that involve other processes and feedback mechanisms (see, for example, [3, 4]). The pre-BötC also interacts with other populations of neurons in the brainstem that are part of the respiratory central pattern generator (CPG) [24], and here too there are advantages in reducing unnecessary complexities [32].

Simplified models of neural systems have been derived using a variety of methods [11]. Activity based models (also known as rate models) of single neurons have been used in [32] to represent populations of neurons in the CPG including the pre-BötC. An activity based model of the pre-BötC neural population was also used in [3, 4]. In all these cases the simplified (phenomenological) models were inspired by models of nonspiking neurons in which bursting becomes a periodic solution and spiking an equilibrium. The parameters were chosen such that certain aspects of the dynamics seen experimentally were captured (such as the change in the bursting frequency), but no attempt was made to check whether the nature and location of bifurcations exhibited by these models do represent the real system (or a more detailed computational model). Capturing such transitions adequately in a simplified model is important when studying breathing patterns that involve repeated transitions from breathing to not breathing (one such instance that requires the study of breathing control at the systems level is Cheyne–Stokes respiration, usually seen during sleep, in people with heart failure as well as in people with neurological disorders, in premature and full term infants, and in healthy people at high altitude [3, 4, 9, 29]).

The transitions from quiescent to bursting to spiking states in a single cell and in a two-cell network were analyzed in [5] by using slow-fast decomposition and averaging over the periodic solutions of the fast subsystem. The transitions are seen in [5] (following [40]) as a shift in the intersection point between the nullcline of the slow variable and the bifurcation diagram of the fast subsystem, in which the slow variable is taken as the bifurcation parameter. When the transition is from quiescent to bursting, the intersection point occurs at a saddle-node bifurcation (the intersection point moves from the lower, stable equilibrium branch of the fast subsystem to the middle, unstable equilibrium branch of the fast subsystem). When the transition is from bursting to spiking, the intersection point occurs at a homoclinic bifurcation

Copyright © by SIAM. Unauthorized reproduction of this article is prohibited.

Downloaded 12/19/19 to 128.112.173.161. Redistribution subject to SIAM license or copyright; see http://www.siam.org/journals/ojsa.php

(where a stable periodic solution of the fast subsystem collides with a saddle-type equilibrium of the fast subsystem located on the middle equilibria branch of the fast subsystem; see also [25]). Although this seems to give good estimates of the parameter values where the transitions occur, the analysis may not be strictly valid, as near the transition from quiescent to bursting, the full system undergoes a Hopf bifurcation (see Figure 1) and therefore has two eigenvalues with zero real parts, and so could potentially have at least two slow variables, not just one as assumed in [5] for a single cell (see also [6]). It is also not clear whether the analysis is strictly valid near the transition from bursting to spiking, and it may well be (as we argue in this paper) that due to the chaotic nature of the spiking and bursting near the transition, this "transition point" may not be well defined. The slow-fast decomposition and averaging techniques have been used to study the transition from quiescent to bursting to spiking in other systems as well (see, for example, [34, 35]), and it has been shown in [1] using several other computational techniques that the bursting and spiking regions in the Hindmarsh–Rose model are separated by multiple layers of chaotic regions that give rise to spike-adding cascades. However, the question of what the "effective" bifurcation points of a simplified model ought to be and how they should correspond to the transitions of the detailed model remain unanswered.

In this paper we strive to address the following question: Could the transitions from the quiescent to bursting to spiking in the full model be represented qualitatively, in a coarse-grained way, so that they appear consistent with a two-dimensional (2D) smooth model? This question is motivated by the modelling needs described above for the pre-BötC. We begin our discussion with a model of a single neuron that consists of three ordinary differential equations (see section 2). This enables us to explain our approach and validate it. We show that in principle the system could be simplified using two ordinary differential equations. Although we can specify the two variables of the simplified system, we cannot write down the equations that describe this model explicitly. Nevertheless, we show in section 3 that the information provided by the two variables of the simplified model can be used to initialize and run a consistent simulation of the original three-dimensional (3D) system, hence providing a mechanism for moving between one model description to another. We then show in section 4 how we can use the equation-free approach [18, 45] to rationalize the type of bifurcations the simplified model should exhibit. Finally, we show in section 5 how the method can be extended to a network of several neurons. The end result of our calculations is not a set of equations for the simplified model but rather a set of properties that should be embodied in such a model.

2. The detailed system and its coarse simplification. The equations of the detailed system of a single neuron in the pre-BötC have the form

$$\begin{aligned} \dot{v} &= f_1(v,n,h), \\ \dot{n} &= f_2(v,n), \\ \dot{h} &= f_3(v,h), \end{aligned} \tag{1}$$

where v is the voltage across the neuron membrane, n is the gating of potassium, h is the gating of persistent sodium, and f_1, f_2, f_3 are specific functions (see Appendix A for more

Copyright © by SIAM. Unauthorized reproduction of this article is prohibited.

Downloaded 12/19/19 to 128.112.173.161. Redistribution subject to SIAM license or copyright; see http://www.siam.org/journals/ojsa.php

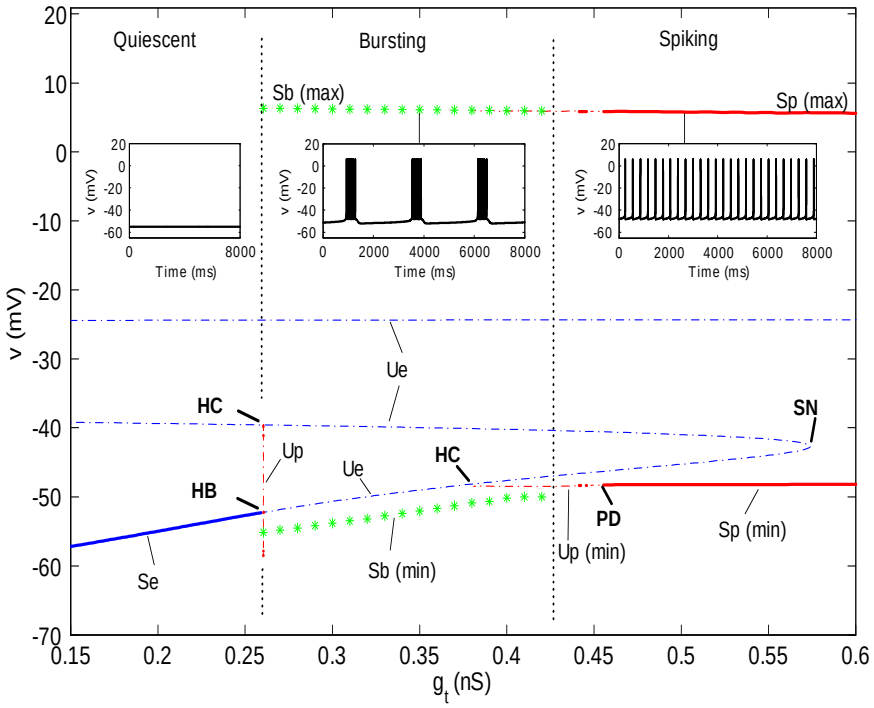

Figure 1. *A typical, partial, bifurcation diagram of a single neuron (based on a model by Butera, Rinzel, and Smith [7]; see Appendix A for more details). V is the voltage across the neuron membrane, and g_t is the bifurcation parameter. The blue solid line is a stable equilibrium (marked with "Se"), the blue dashed-dotted lines are unstable equilibria (marked with "Ue"), the red solid lines show the minimum and maximum of a stable periodic solution (marked with "Sp"), the red dashed-dotted lines show the minimum and maximum of unstable periodic solutions (marked with "Up"), and the green stars show the minimum and maximum of a stable bursting solution (marked with "Sb"). HC - homoclinic bifurcation, PD - period doubling, SN - saddle-node bifurcation. The vertical dotted lines show a qualitative boundary between the three main rhythm states, and the inserts at the top show a typical time series for that state. All the stationary and periodic solutions in the bifurcation diagram were computed using AUTO. The bursting solutions were calculated by direct simulation.*

details). Figure 1 shows the three states (quiescent, bursting, and spiking) in a typical, partial bifurcation diagram of this system.[1] The bifurcation parameter in Figure 1 (g_t) is the conductance of a current representing external control inputs from other areas of the brainstem. It can be seen in Figure 1 that for large parameter values the spiking corresponds to a stable periodic solution. However, at $g_t \approx 0.45$ nS the periodic solution undergoes a period doubling bifurcation and becomes unstable. As g_t is further reduced, more period doubling bifurcations follow (not shown in Figure 1), eventually the spiking becomes chaotic, and at some (subjective) point bursting appears. The minimum and maximum values of the

[1]The bursting solutions in Figure 1 were calculated by direct simulation. All the stationary and periodic solutions in the bifurcation diagram were computed using AUTO. Whenever we refer to AUTO in this paper we mean auto07p-0.8, which is available online from http://cmvl.cs.concordia.ca/auto.

Copyright © by SIAM. Unauthorized reproduction of this article is prohibited.

Downloaded 12/19/19 to 128.112.173.161. Redistribution subject to SIAM license or copyright; see http://www.siam.org/journals/ojsa.php

bursting signal are shown as green stars in Figure 1. As g_t decreases, the number of spikes per burst increases. This transition of "spike adding" may involve chaotic behavior over a small range of parameter values [1, 11, 39, 40]. Around $g_t \approx 0.26$ nS, the bursting disappears and a stable quiescent solution appears. Unstable equilibria coexist with all the different types of solutions seen in Figure 1, and other bifurcation points such as homoclinic and saddle nodes of equilibria also exist.

When considering how to simplify this system, we make the following two observations: (1) the variable h is much slower than the other two variables of the detailed system (at least for some parameter values within the bursting region), and hence it will be natural to expect that this property could be exploited to reduce the system; and (2) the detailed system exhibits oscillatory behavior in the bursting region, and hence it will be natural to expect that a simplified model should be able to capture these oscillations. Both observations were used to simplify this system in the past using different approaches (see the introduction). The first observation led to a slow-fast decomposition analysis of this system and to a simplification of the bursting region in a form of a one-dimensional (1D) discontinuous model (see, for example, [5]), but the resulting simplification could not be easily coupled to models of other subsystems that interact with the pre-BötC. The second observation led to the development of models that consisted of two differential equations, inspired by nonspiking neurons (see, for example, [3, 4, 32]). These 2D models could be considered as phenomenological and ad hoc, as they were derived by removing the equation for n along with the currents I_K and I_{Na} in the equation for v, leading to the following equations:

$$\begin{aligned} c\frac{dv}{dt} &= -I_{NaP} - I_L - g_t v, \\ \frac{dh}{dt} &= \alpha_h(1-h) - \beta_h h, \end{aligned} \tag{2}$$

where c and g_t are parameters, I_L, α_h, and β_h are functions of v, and I_{NaP} is a function of both v and h (see Appendix A for more details). Figure 2 shows the bifurcation diagram generated by (2) and calculated by AUTO with g_t as the bifurcation parameter (this is the same parameter as in Figure 1). The ad hoc model (2) has stable equilibria (solid blue lines) roughly in regions where the 3D model has equilibria and spiking solutions, and stable periodic solutions (solid red lines) roughly for parameter values where bursting is observed. A "proper" reduction where n is assumed to be a fast variable, in a quasi-steady state, leads to the following equations:

$$\begin{aligned} c\frac{dv}{dt} &= -I_{NaP} - I_{Na} - I_k - I_L - g_t v, \\ \frac{dh}{dt} &= \alpha_h(1-h) - \beta_h h, \end{aligned} \tag{3}$$

where I_{Na} and I_k are functions of v (taking $n = \alpha_n/(\alpha_n + \beta_n)$ in the expressions given in Appendix A) and all other parameters and variables are as before. This simplification results in *a very different bifurcation diagram* shown in Figure 3. Here the simplified model has no stable periodic solutions. Instead it has stable equilibria (solid blue lines) that coexist for some parameter values, unlike the 3D model.

Copyright © by SIAM. Unauthorized reproduction of this article is prohibited.

Downloaded 12/19/19 to 128.112.173.161. Redistribution subject to SIAM license or copyright; see http://www.siam.org/journals/ojsa.php

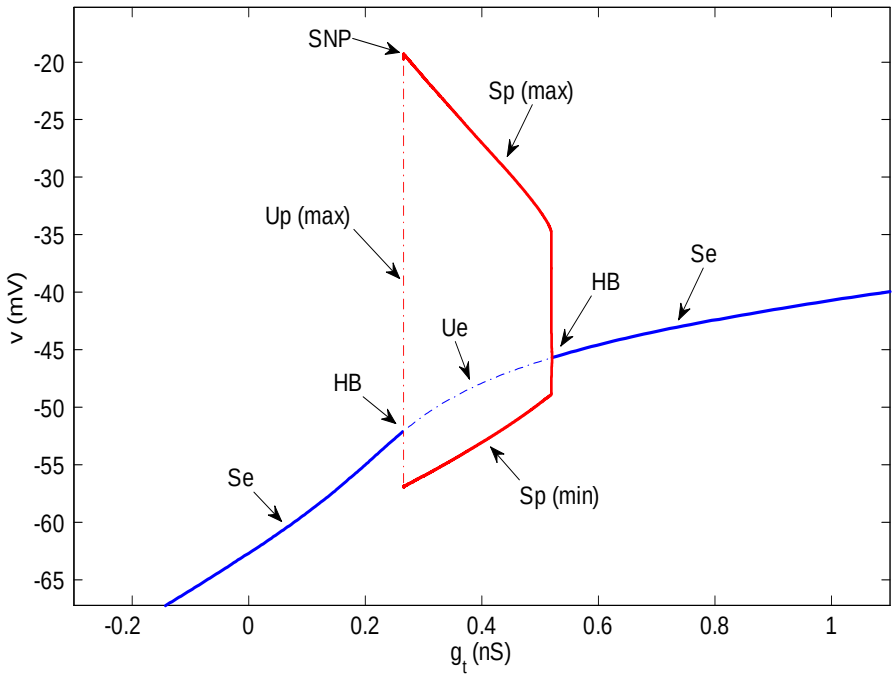

Figure 2. *A bifurcation diagram of an ad hoc model (2). The blue solid line is a stable equilibrium (marked with "Se"), the blue dashed-dotted line is an unstable equilibrium (marked with "Ue"), the red solid line shows the minimum and maximum of a stable periodic solution (marked with "Sp"), and the red dashed-dotted line shows the minimum and maximum of an unstable periodic solution (marked with "Up"). HB - Hopf bifurcation, SNP - Saddle node of periodic solutions. The bifurcation diagram was computed using AUTO.*

One of the difficulties in coupling models at different levels of description is the fact that models at the level of the pre-BötC are based on experiments in rats (and other small mammals) that are done in vitro (in a dish) and in situ (where part of the animal is intact), while models of the integrated system are compared with experiments in living humans. This means that the models need to be scaled before they can be coupled (as, among other things, different species have different breathing rates). Ideally, one would like to have a simplified, easy to scale, 2D continuous model that is linked more closely than previous 2D ad hoc models to the 3D system and hence captures the main features of the dynamics in the mammalian pre-BötC. It is desirable for such a model to represent the bursting as a periodic solution and the spiking as an equilibrium point, but it remains to determine how to represent the different bifurcations that the 3D model exhibits, as certain bifurcations (such as period doubling) that exist in the 3D model cannot exist in a continuous 2D model. In tackling this challenge, then, we make a distinction between two problems: (1) If we were to simplify the system given by (1) using two ordinary differential equations, what should the variables be? (2) What type of bifurcations should the 2D simplified model exhibit so that they rationally correspond to the detailed bifurcation scenario of the 3D model? The first question is addressed in the next section as part of the discussion on the equation-free approach. The second question is addressed

Copyright © by SIAM. Unauthorized reproduction of this article is prohibited.

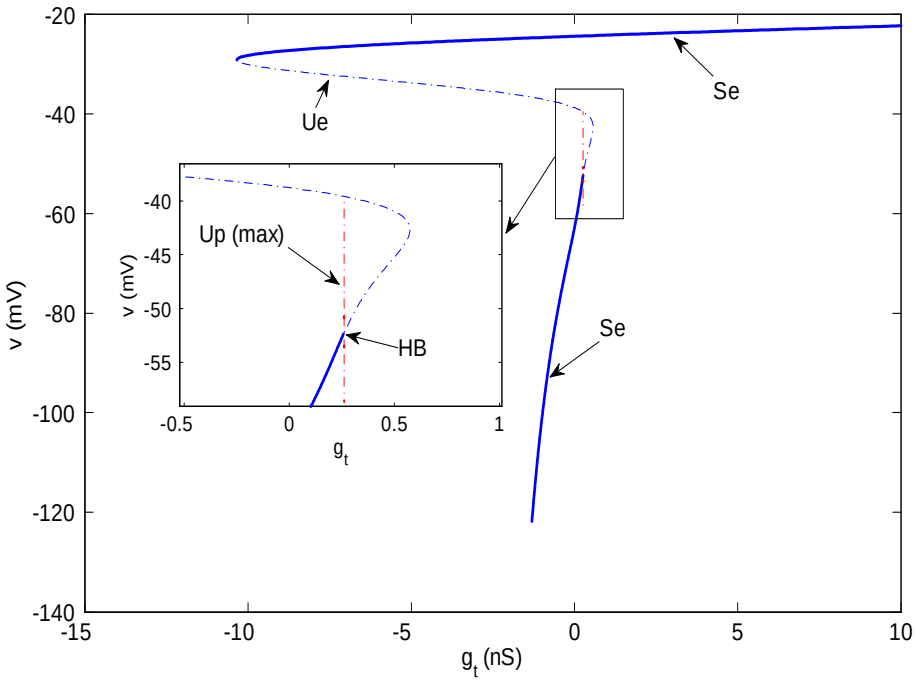

Figure 3. *A bifurcation diagram of a reduction where n is assumed to be a fast variable in a quasi-steady state (3). The blue solid line is a stable equilibrium (marked with "Se"), the blue dashed-dotted line is an unstable equilibrium (marked with "Ue"), and the red dashed-dotted line shows the minimum and maximum of an unstable periodic solution (marked with "Up"). HB - Hopf bifurcation. The bifurcation diagram was computed using AUTO.*

in section 4, where the equation-free approach is used to perform continuation/bifurcation calculations for the simplified model.

3. The equation-free approach.

The idea behind the equation-free (EF) approach is to find a mapping between the variables of a detailed system for which the equations are known (in this case, a bursting neural network) and the variables of a simplified model for which the equations are in principle unknown. The mapping from the detailed system to the simpler, coarse-grained one is called a *restriction operator*, and the reverse (one to many) mapping from the simplified system to a consistent realization of the detailed system is called a *lifting operator* [18]. By moving back and forth between the variables of the detailed neural network and the variables of the simplified system using the restriction and lifting operators, and simulating the detailed neural network for short periods of time, we can calculate the steady states of the simplified model and their stabilities and create bifurcation diagrams for the simplified model even though the equations of the simplified model are unknown. The main difficulty in applying the EF approach, then, is to decide what the relevant coarse variables should be and to construct appropriate restriction and lifting operators. The restriction operator we propose here is obtained by adding a new differential equation to the system.

Copyright © by SIAM. Unauthorized reproduction of this article is prohibited.

Downloaded 12/19/19 to 128.112.173.161. Redistribution subject to SIAM license or copyright; see http://www.siam.org/journals/ojsa.php

The additional differential equation does not change the original problem, but we believe that it helps simplify it.[2]

3.1. The restriction operator for a single neuron. As mentioned above, the restriction operator maps the variables of the detailed system onto the variables of the simplified system. Since the detailed system shows oscillatory behavior in the bursting region, a simplified (smooth) system should have at least two variables. One of the two variables could be h, as this variable is much slower than the other two variables of the detailed system (at least for some parameter values within the bursting region) and exhibits a simpler oscillatory behavior. To find a second slow variable we start by introducing an additional differential equation that augments the detailed system. This idea may appear strange at first—instead of simplifying the system we just made it more complex; however, the usefulness of this approach will be demonstrated shortly. The additional equation is

$$\dot{A} = \alpha(g(v) - A), \tag{4}$$

where

$$g(v) = \frac{1}{1 + e^{-\beta(v-\theta)}} \tag{5}$$

and α, β, and θ are parameters. If $v \ll \theta$, $g(v) \approx 0$. If $v \gg \theta$, $g(v) \approx 1$. β determines how fast the function g moves between 0 and 1, and α is chosen such that A, the new variable, is slower than v. If the value of α is small enough, A is a scaled average of v over time and could be thought of as a measure of the neuron activity: the values of A rise when the neuron is active and fall when the neuron is inactive (see Figure 4). The variables of the detailed system are now v, n, h, and A, and we select the variables of the simplified system to be h and A. If we want to map between the variables of the detailed system at time T and the variables of the simplified system at that time, we simply pick $h(T)$ and $A(T)$.

It might be tempting to use the traditional slow-fast decomposition to derive the equations of the simplified system. If we proceed in this way assuming that v and n are the fast variables and therefore at quasi-steady state near the slow manifold $f_1(v, n, h) \simeq 0$ and $f_2(v, n) \simeq 0$, we get equations of the form $\dot{h} = \tilde{f}_3(h)$ and $\dot{A} = \tilde{f}_4(A, h)$, where $\tilde{f}_3(h)$ and $\tilde{f}_4(A, h)$ are functions which, depending on f_1 and f_2, could sometimes be obtained explicitly. Such a system could never exhibit oscillatory behavior (assuming that $\tilde{f}_3$ is continuously differentiable and the solution is unique). It is therefore not easy to obtain explicit, closed-form approximate equations for the simplified ("coarse") system:

$$\begin{aligned} \dot{h} &= f_{s1}(h, A), \\ \dot{A} &= f_{s2}(h, A), \end{aligned} \tag{6}$$

[2]This "adding so that we can then reduce" is reminiscent of an old riddle about three brothers who inherited 17 camels and had to divide them according to their father's will. The oldest brother was to get a half, the second brother was to get a third, and the youngest was to get a ninth of the camels. An argument arose between the brothers on how the camels should be divided until a passerby gave one of his camels to the brothers. Now that there were 18 camels, it was easy to divide them. The oldest son got nine camels, the second son got six, and the youngest got two. Since $2 + 6 + 9 = 17$, the stranger got his camel back. The new differential equation we add when we construct the restriction operator can be thought of as the 18th camel. We then remove it when we discuss the lifting operator.

Copyright © by SIAM. Unauthorized reproduction of this article is prohibited.

Downloaded 12/19/19 to 128.112.173.161. Redistribution subject to SIAM license or copyright; see http://www.siam.org/journals/ojsa.php

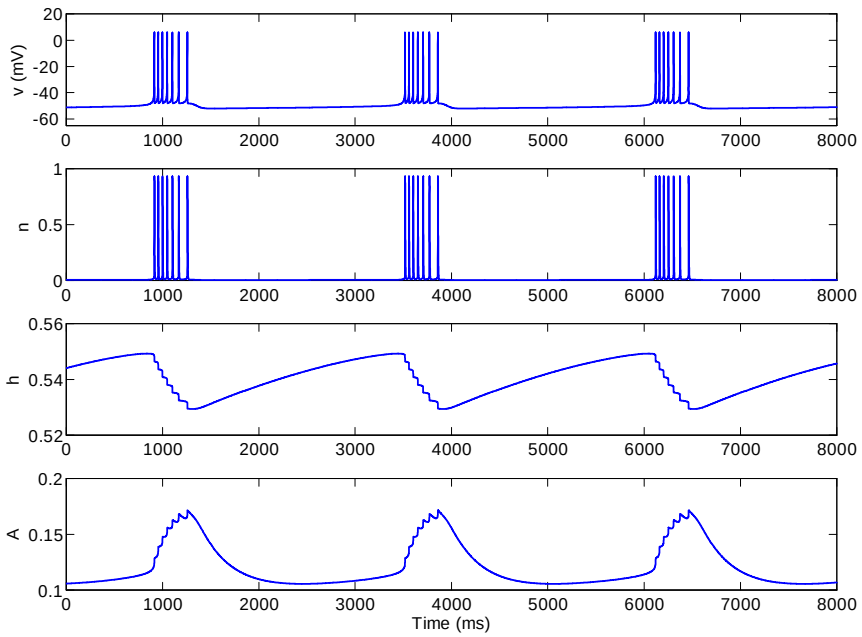

Figure 4. *A bursting solution as seen by the augmented system ((1) and (4), $g_t = 0.35$ [nS], $\alpha = 0.003$ [1/ms], $\beta = 0.1$ [1/mv], and $\theta = -30$ [mv]; other parameters are given in Appendix A). v is the voltage across the neuron membrane, n is the gating of potassium, h is the gating of persistent sodium; A is the additional "observable"; it represents a scaled average of v over time and could be thought of as a measure of the neuron activity.*

where $f_{s1}(h, A)$ and $f_{s2}(h, A)$ are unknown functions.

3.2. The lifting operator for a single neuron. The lifting operator estimates appropriate state values for the detailed system at a given time T based solely on the values of $h(T)$ and $A(T)$ (that is, the lifting operator estimates the values of $v(T)$ and $n(T)$ given h and A). By "appropriate" (or "consistent") we mean that if we were to restart a simulation of the detailed system that was stopped at time T, given the values of $h(T)$ and $A(T)$ obtained when the simulation was stopped, and the estimated values of $v(T)$ and $n(T)$ obtained from the lifting operator, the trajectories of $h(t)$ and $A(t)$ for $t > T$ would have been very close (in an appropriate norm) to the trajectories of $h(t)$ and $A(t)$ in an uninterrupted simulation. To illustrate this point and the main idea behind the lifting operator we look first at a simpler example, taken from [18]. Consider the system

$$\begin{aligned} \dot{x}_1 &= -x_1 - x_2 + 2, \\ \dot{x}_2 &= \frac{1}{\varepsilon}\left(x_1^3 - x_2\right) \end{aligned} \tag{7}$$

with $\varepsilon \ll 1$. As can be seen in Figure 5, the trajectory of x_2 converges quickly to the slow manifold (described by $x_2 = x_1^3$), and then both variables move along the slow manifold

Copyright © by SIAM. Unauthorized reproduction of this article is prohibited.

Downloaded 12/19/19 to 128.112.173.161. Redistribution subject to SIAM license or copyright; see http://www.siam.org/journals/ojsa.php

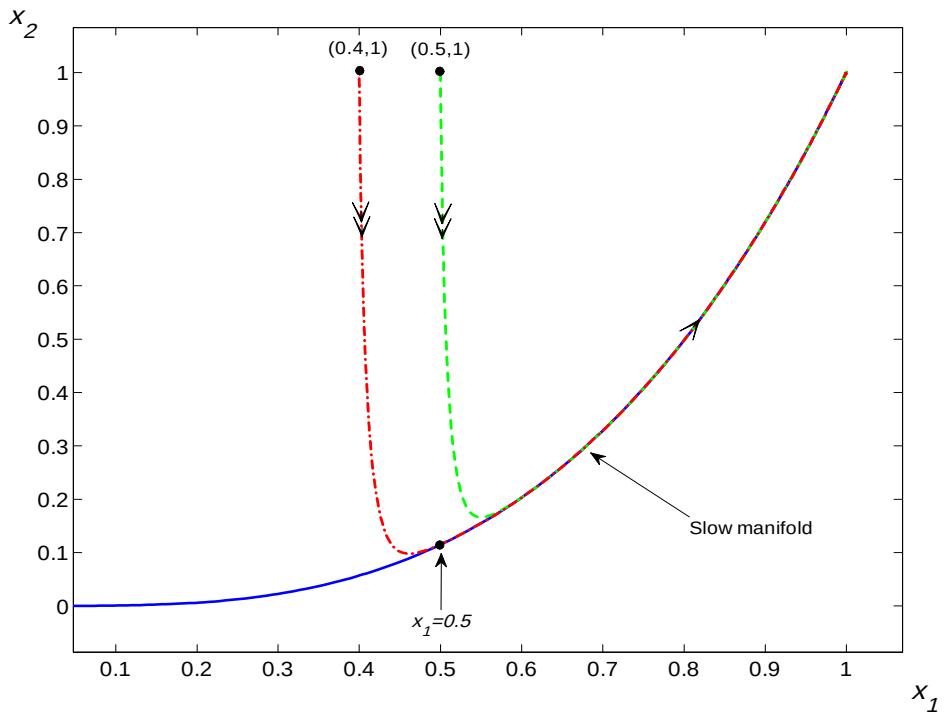

Figure 5. *The main idea behind the lifting operator illustrated in a simple 2D slow-fast system (7). The double arrows indicate the direction of time on the fast manifold.*

towards the steady state $(1, 1)$. In this particular example we can describe the dynamics on the slow manifold by $\dot{x}_1 = -x_1 - x_1^3 + 2$, which is the reduced, "coarse" system. Imagine, however, that the equation for the simplified system is not available in closed form and all we have is the value of x_1 (say, $x_1(T) = 0.5$; see Figure 5). We want to find the value of x_2 on the slow manifold (call it $x_2(T)$). To do this, we fix x_2 at some arbitrary value ($x_2(0) = 1$ in Figure 5), guess a value for x_1 (call it $\tilde{x}_1^1(0)$), and run (7) for a short period of time, τ. We assume that at the end of this short simulation time, x_2 has converged to the slow manifold. We now check the value of x_1 (call it $\tilde{x}_1^1(\tau)$). If it is close enough to 0.5, the lifting is complete: $x_2(\tau)$ is the missing value we need. If $x_1(\tau)$ is too far from 0.5, we guess a new value for $x_1(0)$ (call it $\tilde{x}_1^2(0)$). Guessing a new value for $x_1(0)$ can be performed efficiently using the Newton method (or, in this example, the Steffensen method; more on this below). Finding $x_2(\tau)$ close enough to the slow manifold ensures that if we were to restart the simulation of the system at that point (i.e., near $x_1 = 0.5$, $x_2 = 0.1$), the time evolution of the reduced system would not be visibly altered [45]. The iterative (Newton-type) solution for the initial conditions to be used during the lifting operator makes this an *implicit* lifting (using the terminology proposed in [26] and in the spirit of the lifting algorithms implemented there and in [45]).

We now return our attention to the original system (see (1) and (4)). If it were a standard slow-fast system, we could have fixed the values of the two fast variables and guessed the

Copyright © by SIAM. Unauthorized reproduction of this article is prohibited.

Downloaded 12/19/19 to 128.112.173.161. Redistribution subject to SIAM license or copyright; see http://www.siam.org/journals/ojsa.php

Downloaded 12/19/19 to 128.112.173.161. Redistribution subject to SIAM license or copyright; see http://www.siam.org/journals/ojsa.php

values of the two slow variables, similar to the simple example above. However, (4) is different because the first three equations are independent of A. We could therefore do the following:

1. Fix $v(0)$ and $n(0)$, and guess $h(0)$.
2. Solve (1), and find $h(\tau)$.
3. Check whether $h(\tau)$ is close enough to the desired value $h(T)$.
4. If $h(\tau)$ is not close enough to the desired value, use a solver for nonlinear equations to guess a new $h(0)$ (we used the Steffensen method (see section 3.2.1), but the Newton method could also be used).
5. Repeat steps 2, 3, and 4 if required. Each time step 2 is performed, we also calculate $v(t)$ and $n(t)$ for $0 \le t \le \tau$, so when the Steffensen method converges we also have $v(\tau)$ and $n(\tau)$.

The solution for $v(\tau)$ and $n(\tau)$ found in the steps described above depends strongly on the choice we make for $v(0)$. This is easy to see in the bursting region (see Figure 4), where for almost all given values of $h(\tau)$ some choices of $v(0)$ will lead to values of $v(\tau)$, $n(\tau)$ in the active phase and other choices of $v(0)$ will lead to values of $v(\tau)$, $n(\tau)$ in the silent phase. This is where the information provided by $A(T)$ becomes useful. We know that the values of A rise when the neuron is active and fall when the neuron is inactive; we assume that for the duration of the short time simulation $0 \le t \le \tau$ the neuron is either in the active phase or in the silent phase where the value of A does not change by much. We therefore use the relationship $g(v(0)) = A(T)$ to calculate the value of $v(0)$ in the appropriate state. $n(0)$ is chosen arbitrarily (in all our calculations for a single neuron we used $n(0) = 0.2$).

In addition to the values of $v(\tau)$ and $n(\tau)$, the lifting operator gives us the values of $h(0)$ and $A(0)$. This "by-product" of the lifting operator will be used to calculate fixed points of the simplified system in section 3.3.1. The calculation of $h(0)$ has been described above. To see how $A(0)$ is calculated, observe that the solution of the equation $\dot{A} = \alpha(g(v) - A)$ is given by

$$A(\tau) = e^{-\alpha\tau}\alpha \int_0^\tau e^{\alpha t} g(v(t))\, dt + e^{-\alpha\tau} A(0).$$

Therefore for any given integrable $v(t)$ for $0 \le t \le \tau$ and a given $A(\tau)$ one could find $A(0)$ as

$$A(0) = A(\tau)\, e^{\alpha\tau} - \alpha \int_0^\tau e^{\alpha t} g(v(t))\, dt \equiv A(T)\, e^{\alpha\tau} - \alpha \int_0^\tau e^{\alpha t} g(v(t))\, dt.$$

3.2.1. Improving the guess for $h(0)$. We now show how to use the Steffensen method in a single neuron model to calculate $h(0)$ such that $h(\tau)$ has the desired value $h(T)$. Let $\tilde{h}^j(0)$ be the jth iteration of $h(0)$ and $\tilde{h}^j(\tau)$ the resulting solution after time τ (that is, after (1) was solved). For a single neuron our initial guess is $\tilde{h}^1(0) = h(T)$. Define

$$\tilde{f}\left[\tilde{h}^j(0)\right] \triangleq \tilde{h}^j(\tau) - h(T).$$

Our goal is to find $\tilde{h}^j(0)$ such that $\left|\tilde{f}\left[\tilde{h}^j(0)\right]\right| < \delta$. In all our simulations we set $\delta = 10^{-14}$. Using the Steffensen method we calculate a new guess $\tilde{h}^{j+1}(0)$ as [33]

$$\tilde{h}^{j+1}(0) = \tilde{h}^j(0) - \frac{\tilde{f}^2\left[\tilde{h}^j(0)\right]}{\tilde{f}\left[\tilde{h}^j(0) + \tilde{f}\left[\tilde{h}^j(0)\right]\right] - \tilde{f}\left[\tilde{h}^j(0)\right]}.$$

Copyright © by SIAM. Unauthorized reproduction of this article is prohibited.

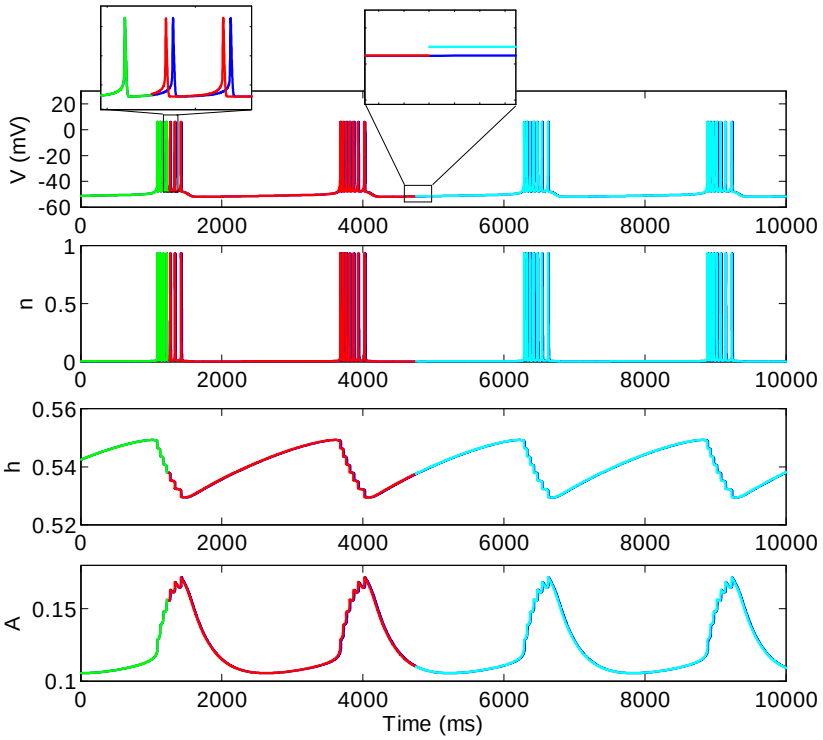

Figure 6. *Examples of successful lifting. The blue line shows an undisturbed simulation. The green line shows the original simulation until it was stopped at $t = 1250$ [ms]. The red and cyan lines show the simulation after the lifting operator was used at $t = 1250$ and $t = 4750$ [ms], respectively (the inserts show a closer view near these points). v is the voltage across the neuron membrane, n is the gating of potassium, h is the gating of persistent sodium, and A is a measure of the neuron activity. $g_t = 0.35$ [nS], $\alpha = 0.003$ [1/ms], $\beta = 0.1$ [1/mv], $\theta = -30$ [mv], and $\tau = 60$ [ms]; other parameters are given in Appendix A.*

The Steffensen method is of the same order as the Newton method (which could have been used here instead) but does not require an evaluation of the derivative. We do, however, evaluate the function twice (once at $\tilde{h}^j(0)$ and once at $\tilde{h}^j(0) + \tilde{f}[\tilde{h}^j(0)]$). Note also that the Steffensen method, unlike the Newton method, can only be applied to scalar functions [33].

3.2.2. Examples of successful and unsuccessful lifting. Figure 6 shows two examples of successful lifting. The blue line shows an undisturbed simulation. The green line shows the original simulation until it was stopped at $t = 1250\ ms$. The red and cyan lines show the simulation after the lifting operator was used at $t = 1250$ and $t = 4750\ ms$, respectively. To test the lifting operator, only the values of h and A were retained. That is, the values of $h(1250)$, $A(1250)$ and $h(4750)$, $A(4750)$ were used to estimate the values of $v(1250)$, $n(1250)$ and $v(4750)$, $n(4750)$. The inserts show a closer view near these points. Although the time series of $v(t)$ and $n(t)$ are not followed perfectly, the time series of $h(t)$ and $A(t)$ are undisturbed. This can also be seen in Figure 7, where the two examples of successful lifting are shown in phase plane.

An example of an unsuccessful lifting is shown in Figure 8. The blue line shows an undisturbed simulation. The green line shows the original simulation until it was stopped

Copyright © by SIAM. Unauthorized reproduction of this article is prohibited.

Downloaded 12/19/19 to 128.112.173.161. Redistribution subject to SIAM license or copyright; see http://www.siam.org/journals/ojsa.php

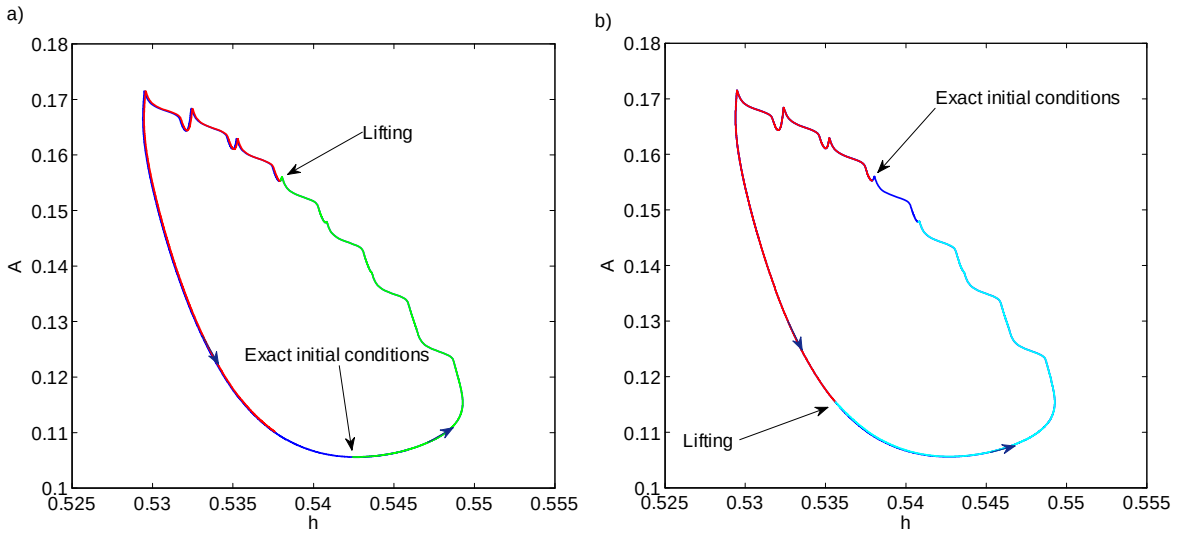

Figure 7. *Examples of successful lifting in the phase plane. In both graphs, the blue line shows an undisturbed simulation and the blue arrows indicate the direction of time.* (a) *The green line shows the original simulation until it was stopped at the active phase, and the red line shows the simulation after the lifting operator was used.* (b) *The red line shows the original simulation until it was stopped at the quiescent phase, and the cyan line shows the simulation after the lifting operator was used. The variables and parameters are the same as in Figure 6.*

at $t = 3600\ ms$. The red line shows the simulation after the lifting operator was used at $t = 3600\ ms$ (that is, the values of $h(3600)$, $A(3600)$ were used to estimate the values of $v(3600)$, $n(3600)$; the insert shows a closer view near this point). Here the detailed system is very sensitive to small changes in the values of its variables and the time series of $h(t)$ and $A(t)$ are not estimated well enough (see also Figure 9). The assumption that the neuron is either in the active state or in the quiescent state does not hold in this particular example.

3.3. Calculating stationary simplified solutions and their stability. One of the advantages of the numerical approach we propose in this paper is that it enables us to calculate the stability of stationary simplified solutions even though we do not have the equations of the simplified system. This gives us important information about the type of bifurcation the simplified system undergoes which would not necessarily be available through direct simulations. Recall that the lifting operator enabled us to find the missing values $v\,(T)$ and $n\,(T)$ which are needed (together with $h\,(T)$ and $A\,(T)$ that we kept) if we wish to restart a simulation of the detailed system at some point $t = T$. But the lifting operator also resulted in the calculations of $h(0)$ and $A\,(0)$. We can now use these additional results to calculate the stationary solutions of the simplified system directly and obtain information about the stabilities of these solutions. We first define a stationary solution as a solution where $|h(\tau) - h(0)| < \delta$ and $|A(\tau) - A(0)| < \delta$, where δ is a small number. This definition allows us to regard an oscillating solution with very small amplitude as "coarsely stationary." We can now guess the values of a stationary solution (call it h^1, A^1) and set them as the desired values for $h(\tau)$, $A\,(\tau)$. We

Copyright © by SIAM. Unauthorized reproduction of this article is prohibited.

Downloaded 12/19/19 to 128.112.173.161. Redistribution subject to SIAM license or copyright; see http://www.siam.org/journals/ojsa.php

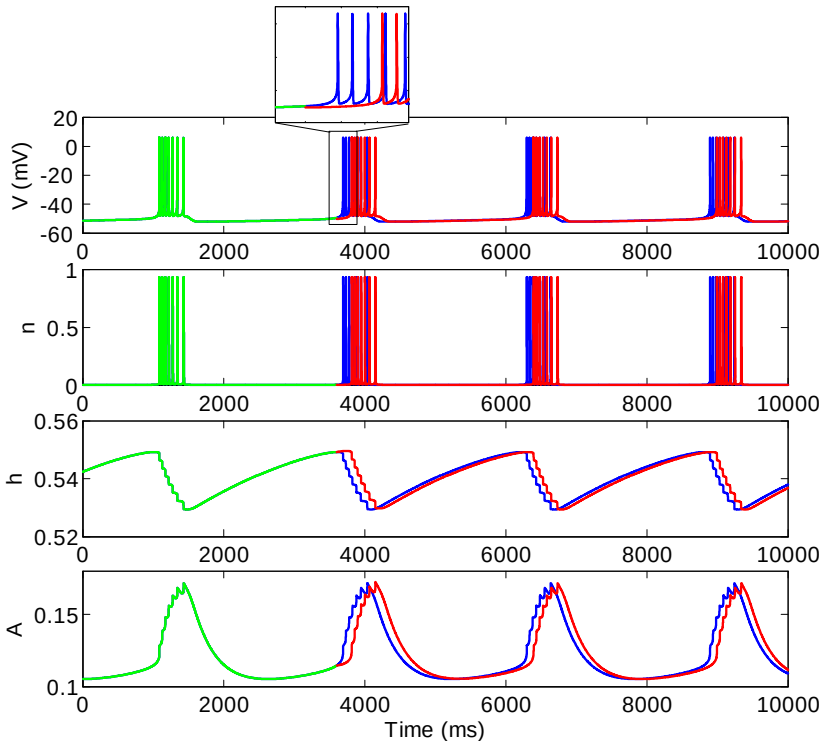

Figure 8. *Example of an unsuccessful lifting. The blue line shows an undisturbed simulation. The green line shows the original simulation until it was stopped at $t = 3600$ [ms]. The red line shows the simulation after the lifting operator was used at $t = 3600$ [ms]. The insert shows a closer view near this point. Here the detailed system is very sensitive to small changes in the values of the variables. v is the voltage across the neuron membrane, n is the gating of potassium, h is the gating of persistent sodium, and A is a measure of the neuron activity. $g_t = 0.35$ [nS], $\alpha = 0.003$ [1/ms], $\beta = 0.1$ [1/mv], $\theta = -30$ [mv], and $\tau = 60$ [ms]; other parameters are given in Appendix A.*

then use the lifting operator to calculate $h(0)$, $A(0)$ and check whether the conditions for a stationary solution are satisfied. If not, we refine our guess for a stationary solution using the Newton method, as we now explain in more detail.

3.3.1. Newton method for the simplified system.

Define

$$\begin{aligned} g_1\left[h(\tau), A(\tau)\right] &\triangleq h(\tau) - h(0), \\ g_2\left[h(\tau), A(\tau)\right] &\triangleq A(\tau) - A(0). \end{aligned} \tag{8}$$

Here we assume that the desired values have already been assigned to $h(\tau)$, $A(\tau)$ and note that both will affect the values of $h(0)$ and $A(0)$ in g_1 and g_2, respectively, via the lifting operator (recall that the value of $v(0)$ is calculated from $A(\tau)$, which in turn affects the value of $h(0)$, and the value of $A(0)$ is calculated from $v(t)$, which is affected by the value of $h(\tau)$). We would like to find $h(\tau)$, $A(\tau)$ such that $|g_1\left[h(\tau), A(\tau)\right]| < \delta$ and $|g_2\left[h(\tau), A(\tau)\right]| < \delta$.

Let $h^j(\tau)$, $A^j(\tau)$ be the jth guess of a stationary solution and $h^j(0)$, $A^j(0)$ the output of the lifting operator at that iteration. If $\left|g_1\left[h^j(\tau), A^j(\tau)\right]\right| > \delta$ or $\left|g_2\left[h^j(\tau), A^j(\tau)\right]\right| > \delta$, we

Copyright © by SIAM. Unauthorized reproduction of this article is prohibited.

Downloaded 12/19/19 to 128.112.173.161. Redistribution subject to SIAM license or copyright; see http://www.siam.org/journals/ojsa.php

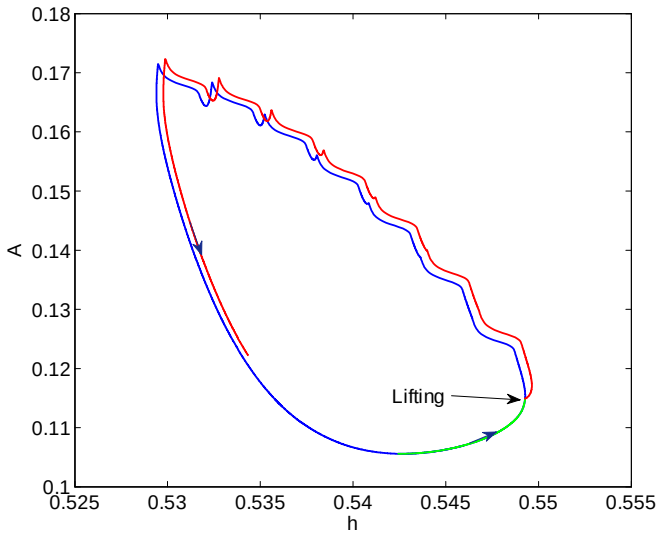

Figure 9. *Example of unsuccessful lifting in phase plane. The blue line shows an undisturbed simulation, the green line shows the original simulation until it was stopped, and the red line shows the simulation after the lifting operator was used. The blue arrows indicate the direction of time. The variables and parameters are the same as in Figure 8.*

find a new guess $h^{j+1}(\tau)$, $A^{j+1}(\tau)$ by using Newton's method [33]:

$$J\left[h^j(\tau), A^j(\tau)\right]\left[\begin{pmatrix} h^j(\tau) \\ A^j(\tau) \end{pmatrix} - \begin{pmatrix} h^{j+1}(\tau) \\ A^{j+1}(\tau) \end{pmatrix}\right] = \begin{pmatrix} g_1\left[h^j(\tau), A^j(\tau)\right] \\ g_2\left[h^j(\tau), A^j(\tau)\right] \end{pmatrix},$$

where

$$J\left[h^j(\tau), A^j(\tau)\right] = \begin{bmatrix} J_{11} & J_{12} \\ J_{21} & J_{22} \end{bmatrix}$$

is the Jacobian with elements estimated through finite difference operations:

$$J_{11} = \frac{g_1\left[h^j(\tau)+\varepsilon,\, A^j(\tau)\right] - g_1\left[h^j(\tau),\, A^j(\tau)\right]}{\varepsilon}, \quad J_{12} = \frac{g_1\left[h^j(\tau),\, A^j(\tau)+\varepsilon\right] - g_1\left[h^j(\tau),\, A^j(\tau)\right]}{\varepsilon},$$
$$J_{21} = \frac{g_2\left[h^j(\tau)+\varepsilon,\, A^j(\tau)\right] - g_2\left[h^j(\tau),\, A^j(\tau)\right]}{\varepsilon}, \quad J_{22} = \frac{g_2\left[h^j(\tau),\, A^j(\tau)+\varepsilon\right] - g_2\left[h^j(\tau),\, A^j(\tau)\right]}{\varepsilon},$$

with ε being a small number (usually we choose $\varepsilon = 10^2\delta$). The eigenvalues of $J\left[h(\tau), A(\tau)\right]$ can be used to evaluate the stability of the unknown system (6).

Let $\mathbf{x}$ denote the perturbation of $[h, A]^T$ from equilibrium. Then near equilibrium we have

$$\dot{\mathbf{x}} = \mathbf{D}_{\mathbf{f}s}\mathbf{x},$$

where

$$\mathbf{D}_{\mathbf{f}s} = \begin{bmatrix} \frac{\partial f_{s1}}{\partial h} & \frac{\partial f_{s1}}{\partial A} \\ \frac{\partial f_{s2}}{\partial h} & \frac{\partial f_{s2}}{\partial A} \end{bmatrix}.$$

Copyright © by SIAM. Unauthorized reproduction of this article is prohibited.

Downloaded 12/19/19 to 128.112.173.161. Redistribution subject to SIAM license or copyright; see http://www.siam.org/journals/ojsa.php

Downloaded 12/19/19 to 128.112.173.161. Redistribution subject to SIAM license or copyright; see http://www.siam.org/journals/ojsa.php

We can now write

$$\mathbf{g} = \mathbf{x}(\tau) - \mathbf{x}(\mathbf{0}) = \mathbf{e}^{\mathbf{D_{fs}}\tau}\mathbf{x}(\mathbf{0}) - \mathbf{x}(\mathbf{0}) = \mathbf{x}(\tau) - \mathbf{e}^{-\mathbf{D_{fs}}\tau}\mathbf{x}(\tau),$$

which leads to

$$J[\mathbf{g}] = \mathbf{I} - \mathbf{e}^{-\mathbf{D_{fs}}\tau}.$$

Let $\tilde{\lambda}_i$ be an eigenvalue of $(\mathbf{I}-J[\mathbf{g}])$ and λ_i be an eigenvalue of $\mathbf{D_{fs}}$. Then (assuming $\tilde{\lambda}_i$ are distinct),

$$e^{-\lambda_i\tau} = \tilde{\lambda}_i$$

and

$$\lambda_i = -\frac{\ln(\tilde{\lambda}_i)}{\tau}.$$

3.4. Conclusions for section 3. At the heart of the EF approach lie restriction and lifting operators that map between the variables of a detailed, known system of equations to the variables of a simplified, in principle unknown, system. In section 3.1 we introduced the restriction operator which involved the addition of a new observable to the original system (the variable A), and in section 3.2 we introduced the lifting operator which itself involved time simulations of the detailed system for short periods of time and using the Steffensen method (or the Newton method; see section 3.2.1). The examples we showed in section 3.2.2 were designed to check the quality of the lifting operator and illustrate its limitations. Once we have a working lifting operator we can use it to calculate stationary solutions of the simplified system and their stabilities (section 3.3). This calculation also involves the Newton method but at the level of the simplified system (section 3.3.1). All the results we show next in section 4 are based on calculations of stationary solutions of the simplified system, and the examples we showed in section 3.2.2 are not relevant for this next section of the paper.

4. Results for a single neuron. We are now in a position to attempt answering the question we posed in the introduction: Can the transitions from quiescent to bursting to spiking solutions in a single neuron be coarse-grained (i.e., represented "roughly") in a way that is consistent with a 2D smooth model? We start by observing the dynamics in the detailed (augmented) system (see (1) and (4)), and we then show how by "blurring our vision" (or looking at the bifurcation diagram from a distance), with the help of the EF approach, we can indeed simplify the dynamics.

Figure 10 shows a bifurcation diagram for (1) and (4) as observed for A, the neuron activity measure (see (4)). The bifurcation parameter, g_t, is the conductance of a current representing external control inputs that affect the neuron. As in Figure 1, the blue solid line is a stable equilibrium (marked with "Se"), the blue dashed-dotted line is an unstable equilibrium (marked with "Ue"), the red solid line shows the minimum and maximum of a stable periodic solution (marked with "Sp"; note that the minimum and maximum of the stable periodic solution are close together and can only be distinguished in the insert), and the red dashed-dotted line shows the minimum and maximum of an unstable periodic solution (marked with "Up"). All these lines were calculated using AUTO. The green stars show the minimum and maximum of a stable bursting solution (marked with "Sb"), calculated by direct simulation. As can be seen in Figure 10, the minimum and maximum of the stable periodic

Copyright © by SIAM. Unauthorized reproduction of this article is prohibited.

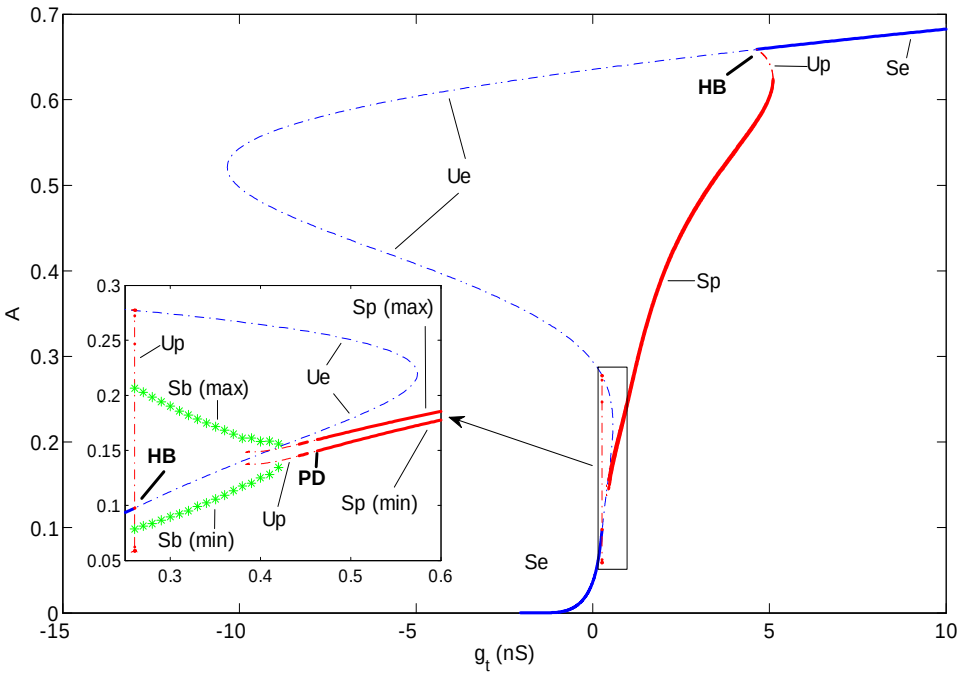

Figure 10. *A partial, bifurcation diagram of the augmented system representing a single neuron (see (1) and (4)). A is the neuron activity measure, and g_t is the bifurcation parameter. The blue solid line is a stable equilibrium (marked with "Se"), the blue dashed-dotted line is an unstable equilibrium (marked with "Ue"), the red solid line shows the minimum and maximum of a stable periodic solution (marked with "Sp"), the red dashed-dotted line shows the minimum and maximum of an unstable periodic solution (marked with "Up"), and the green stars show the minimum and maximum of a stable bursting solution (marked with "Sb"). HC - homoclinic bifurcation, PD - period doubling, SN - saddle-node bifurcation. All the stationary and periodic solutions in the bifurcation diagram were calculated by AUTO. The bursting solutions were calculated by direct simulation. Note that the minimum and maximum of the stable periodic solution are close together and could therefore be thought of as a coarse equilibrium. $\alpha = 0.003$ [1/ms], $\beta = 0.1$ [1/mv], and $\theta = -30$ [mv].*

solution are close together and could therefore be thought of as a coarse equilibrium (this is also true for some of the unstable periodic solutions). The insert in Figure 10 reveals that the maximum and minimum of the bursting solution approach the maximum and minimum of the periodic solution.

Figure 11 shows a projection of several attractors of (1) and (4) into the plane (h, A) for different values of g_t. Between $g_t = 0.26$ nS and 0.28 nS, g_t increases by steps of 0.01 nS and thereafter it increases by steps of 0.02 nS. At $g_t = 0.26$ nS there is a stable equilibrium. At $g_t = 0.27$ nS there is a stable bursting solution which could be viewed as a simple periodic solution in the (h, A) plane. The amplitude of the bursting solution gets smaller continuously as g_t increases, but at $g_t = 0.42$ nS the bursting can no longer be regarded as a simple periodic solution, as the solution crosses itself. The solutions between $g_t = 0.46$ nS and $g_t = 0.5$ nS are stable, simple spiking (by simple we mean period-1; see Figure 10).

We now show a partial bifurcation diagram we created using the reduced variables and the

Copyright © by SIAM. Unauthorized reproduction of this article is prohibited.

Downloaded 12/19/19 to 128.112.173.161. Redistribution subject to SIAM license or copyright; see http://www.siam.org/journals/ojsa.php

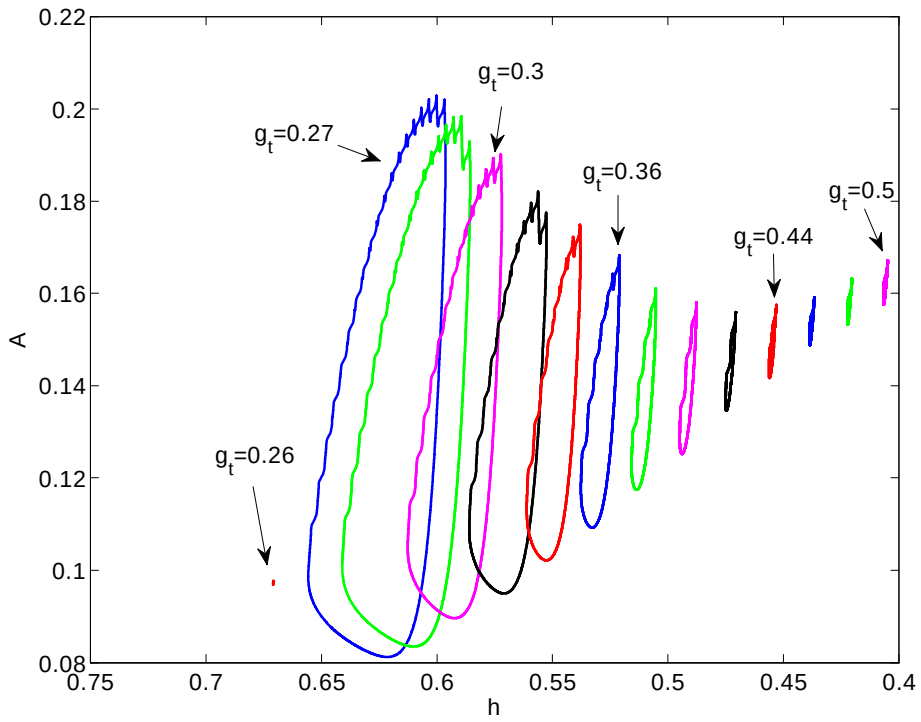

Figure 11. *A projection of several attractors of the detailed system into the plane* (h, A) *(see* (1) *and* (4)*). At* $g_t = 0.26$ *[nS] there is a stable equilibrium, and at* $g_t = 0.27$ *[nS] there is a stable bursting solution which could be viewed as a simple periodic solution in the* (h, A) *plane. Between* $g_t = 0.26$ *[nS] and* 0.28 *[nS],* g_t *grows by* 0.01 *[nS] and thereafter it grows by* 0.02 *[nS]. The solutions between* $g_t = 0.46$ *[nS] and* $g_t = 0.5$ *[nS] are stable, simple spiking (see also Figure* 10*). Note that* h *is decreasing when* g_t *is increasing.*

EF approach (see Figure 12). The rightmost or the leftmost equilibrium points were obtained starting with time simulations of the detailed system whose final points were then used as initial guesses to the Newton method for the simplified system (section 3.3.1). Thereafter, the Newton calculation at each point was used as the initial guess for the next point when g_t was increased or decreased. The green (overlapping) stars in Figure 12 are stable equilibria of the simplified system, and the black circles are unstable equilibria of the simplified system. All the other lines in Figure 12 are the same as in Figure 10. Insert "A" in Figure 12 shows that the Hopf bifurcation for the detailed system can be "bypassed," leading to a connection between the equilibrium and periodic solutions of the detailed system and the consideration of both as belonging to a single branch of stable equilibria in the simplified system. On the other hand, the Hopf bifurcation in insert "C" is also identified as a Hopf bifurcation by the EF approach. The periodic solutions in the simplified system (bursting in the detailed system) are not shown in this figure, to enable a better view of the bifurcation point; however, the transition from bursting to spiking in the detailed system is marked with a dashed green line (note that this transition is not well defined; see the discussion below). Note that our

Copyright © by SIAM. Unauthorized reproduction of this article is prohibited.

Downloaded 12/19/19 to 128.112.173.161. Redistribution subject to SIAM license or copyright; see http://www.siam.org/journals/ojsa.php

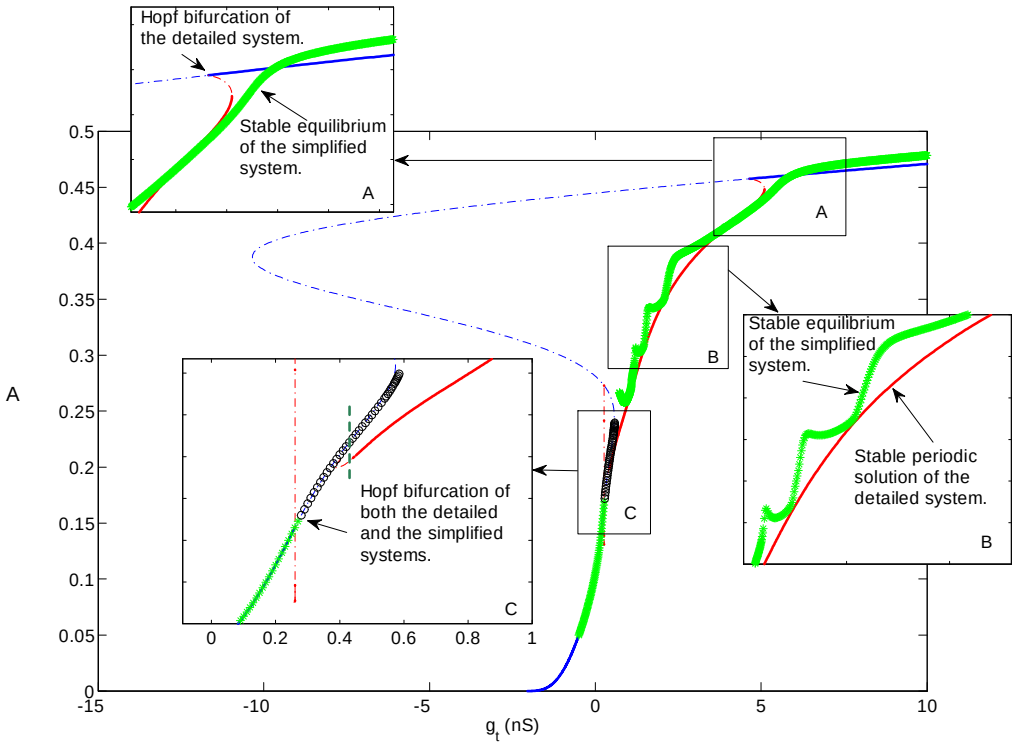

Figure 12. *Using the EF approach to create a partial bifurcation diagram for one cell. Green stars - stable equilibria, black circles - unstable equilibria; both are calculated using the EF approach. Other lines - computed by AUTO using the detailed system; solid blue line - stable equilibria, dashed blue line - unstable equilibria, solid red line - stable periodic, dashed red line - unstable periodic solution.* $\alpha = 0.003$ *[1/ms],* $\beta = 0.05$ *[1/mv],* $\theta = -20$ *[mv], and* $\tau = 30$ *[ms]. The green dashed line in insert "C" indicates where the transition from spiking to bursting occurs (bursting is not shown here, but see Figure 10). This transition is not well defined (see the text for further discussion).*

approach allows us to follow unstable stationary solutions of the simplified system for g_t values close to the Hopf bifurcation. Depending on the values of τ, α, β, and θ, the calculation will eventually either stop converging to a stationary solution or jump to the stable equilibria branch shown in insert "B." Insert "B" shows that the stable periodic solution in the detailed system can still be considered as a stable equilibrium in the simplified system but the tracing of the periodic solution undulates. We discuss the reasons for these undulations and how they can be minimized in subsection 4.2.

Our observations in Figures 10 and 11 as well as the bifurcation diagrams we created using the EF approach in Figure 12 lead us to suggest the schematic bifurcation diagram shown in Figure 13 for a simplified 2D smooth system (we give further justification for this simplified bifurcation diagram later in this section). We suggest that the simplified system undergoes a subcritical Hopf bifurcation near $g_t = 0.26$ nS and that stable periodic solutions appear via a saddle-node bifurcation for periodic solutions. The periodic solutions later terminate via another Hopf bifurcation, and stable equilibria exist for all larger g_t values. The second Hopf

Copyright © by SIAM. Unauthorized reproduction of this article is prohibited.

Downloaded 12/19/19 to 128.112.173.161. Redistribution subject to SIAM license or copyright; see http://www.siam.org/journals/ojsa.php

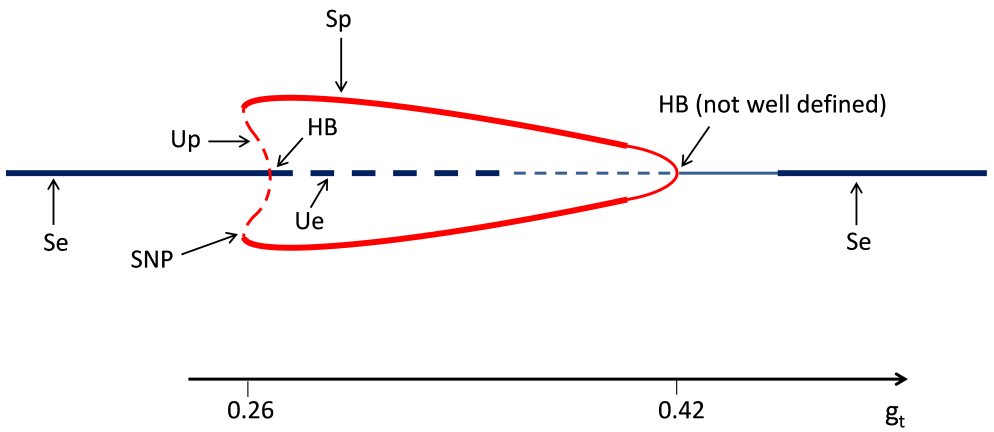

Figure 13. *Schematic description of the bifurcation diagram of the simplified system. Se - stable equilibrium, Ue - unstable equilibrium, Sp - stable periodic solution, Up - unstable periodic solution, HB - Hopf bifurcation, SNP - saddle node of periodic solutions. The thinner lines represent vague solutions where the interpretation of the solutions in the full system is arguable (see the text for further discussion).*

bifurcation, however, is not well defined. We chose it to be near $g_t = 0.42$ nS because this is where a 2D approximation clearly fails (the periodic solution crosses itself). However, deciding when small variations in the values of variables could be considered a "point" and when they should be considered "oscillations" is arbitrary, as is the distinction between chaotic spiking and chaotic bursting (see also [1]).

The simplified bifurcation diagram we propose is similar to the bifurcation diagram obtained from an ad hoc model (Figure 2). The ad hoc model captures two Hopf bifurcations and a stable periodic solution, as in our model. The first Hopf is in the same location as ours (at $g_t \simeq 0.26$ nS), but the second Hopf is further away, at $g_t \simeq 0.52$ nS instead of 0.42 nS. Another difference is the sharp reduction in the amplitude of the periodic solution near the second Hopf bifurcation in the ad hoc model, while we demonstrated that the amplitude reduction is gradual. The "proper" reduction, if n were assumed to be a fast variable in a quasi-steady state (see (3)), yields a very different bifurcation diagram (Figure 3). While the Hopf bifurcation at $g_t \simeq 0.26$ nS is captured, a stable periodic solution does not exist in this reduction. Both of these reductions give further support for the existence of a subcritical Hopf bifurcation at $g_t \simeq 0.26$ nS in the simplified system, but they also illustrate that our results are not trivial.

In the rest of this section we provide further justification for our suggested simplification.

4.1. Justification for ignoring a "detailed" Hopf bifurcation (results in insert "A" of Figure 12). Figure 12 was calculated using $\tau = 30$ ms (this is the length of time for which the detailed system is simulated; see section 3.2). Figure 14 compares the results in insert "A" of Figure 12 with the same calculation using $\tau = 120$ ms (shown in cyan). It shows that the equilibria of the detailed system found by AUTO are followed more closely by our algorithm when $\tau = 120$ ms but the result is the same qualitatively.

Figure 15 shows a simulation of the detailed system upon convergence of the Newton

Copyright © by SIAM. Unauthorized reproduction of this article is prohibited.

Downloaded 12/19/19 to 128.112.173.161. Redistribution subject to SIAM license or copyright; see http://www.siam.org/journals/ojsa.php

Downloaded 12/19/19 to 128.112.173.161. Redistribution subject to SIAM license or copyright; see http://www.siam.org/journals/ojsa.php

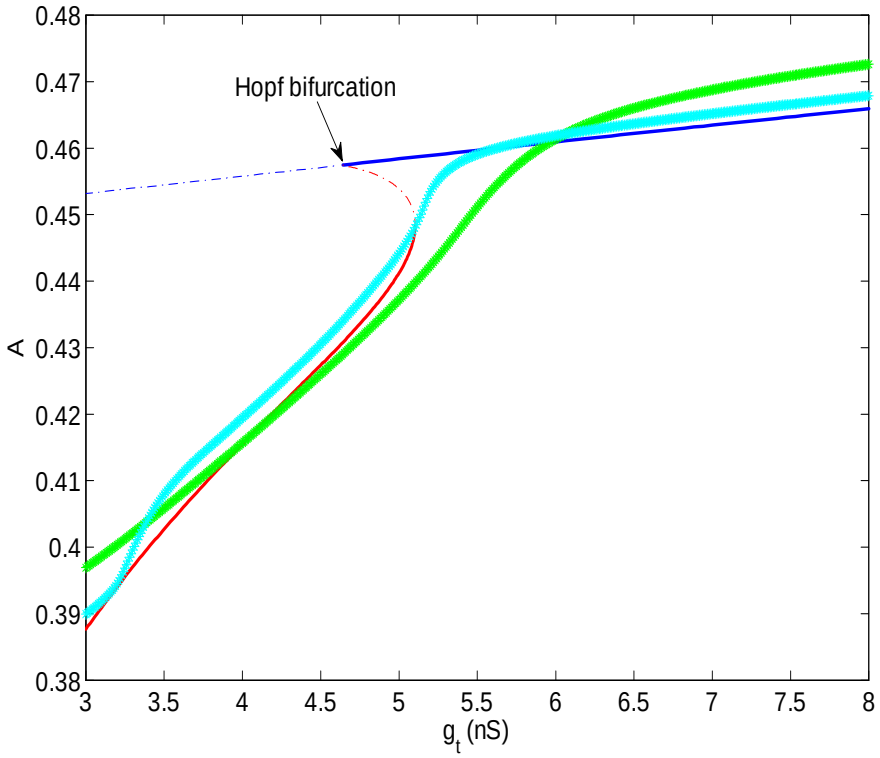

Figure 14. *The Hopf bifurcation of the detailed system can be ignored. A comparison of the EF calculation for two values of τ in insert "A" of Figure 12. Green (overlapping) stars: $\tau = 30$ [ms], cyan (overlapping) stars: $\tau = 120$ [ms].*

method for the simplified system (section 3.3.1). The simulation was done during the last lifting when $\tau = 120$ ms and $g_t = 6$ nS. It shows that the variables of the detailed system oscillate considerably before they converge to steady state (the variables of the simplified system also oscillate but at a much smaller amplitude). Note that the condition $h(\tau) = h(0)$, $A(\tau) = A(0)$ is satisfied. However, it can also be shown (for proof, see section 3.2) that if $A(\tau) = A(0)$, then

$$A(\tau) = \frac{\alpha \int_0^\tau e^{\alpha t} g(v(t))\, dt}{e^{\alpha\tau} - 1}. \tag{9}$$

In other words, the equilibrium of the simplified system reflects the averaged transient oscillations of the detailed system near the attractor. The closer we get to the Hopf bifurcation the more prolonged these transient oscillations are and the more divergent $A(\tau)$ becomes from the equilibrium of the detailed system. Equation (9) also shows that the equilibria of the detailed and simplified systems will be the same if $g(v(t)) = \text{const}$. However, any initialization of the detailed system away from its equilibrium (as is done in the lifting operator) will lead to the oscillations seen in Figure 15 and these integrated oscillations will lead to $A(\tau) = A(0)$ away from the equilibrium of the detailed system.

Copyright © by SIAM. Unauthorized reproduction of this article is prohibited.

Downloaded 12/19/19 to 128.112.173.161. Redistribution subject to SIAM license or copyright; see http://www.siam.org/journals/ojsa.php

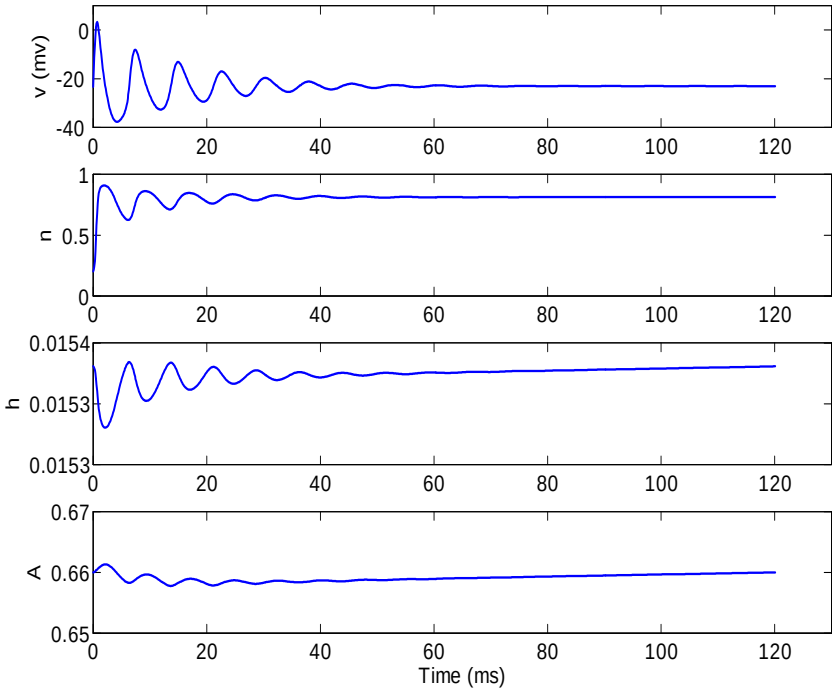

Figure 15. *The divergence of the estimated equilibrium from the original equilibrium reflects the transient behavior of the detailed system. The figure shows a simulation of the detailed system upon convergence of the Newton method for the simplified system (section 3.3.1). The simulation is performed during the last lifting when* $\tau = 120$ *[ms] and* $g_t = 6$ *[nS]. Note that the requirement* $h(\tau) = h(0)$, $A(\tau) = A(0)$ *is met.* v *is the voltage across the neuron membrane,* n *is the gating of potassium,* h *is the gating of persistent sodium, and* A *is a measure of the neuron activity.*

4.2. Justification of the results in insert "B" of Figure 12. Figure 16 compares the results in insert "B" of Figure 12 with the same calculation using $\tau = 120\ ms$ (shown in cyan). It shows that the stable periodic solution for the detailed system (red line) found by AUTO is followed more closely by our algorithm when $\tau = 120\ ms$ but the result is the same qualitatively. Figure 17 compares the time evolution of the system following convergence of the Newton method for the simplified system with the actual steady state of the system when $g_t = 1.7$ nS. It shows that $A(t)$, $h(t)$ converge slowly to the actual steady states and could therefore appear like steady states in the short time simulation of the lifting operator (where $\tau = 30\ ms$). Over this short period of time $v(t)$ has only two action potentials. Recall that the value of $A(\tau) = A(0)$ is calculated by (9) and hence depends on the integral over $e^{\alpha t} g(v(t))$. When g_t is reduced the period of $v(t)$ gets larger (at the same time, $A(t)$, $h(t)$ also converge more slowly to the actual steady state), and hence the integral will be more sensitive to changes in initial conditions of $v(t)$. This explains why the solution in Figure 16 undulates and why the undulations are reduced when τ is increased. When $g_t = 0.6$ nS we need $\tau = 500\ ms$ to capture at least three action potentials.

Copyright © by SIAM. Unauthorized reproduction of this article is prohibited.

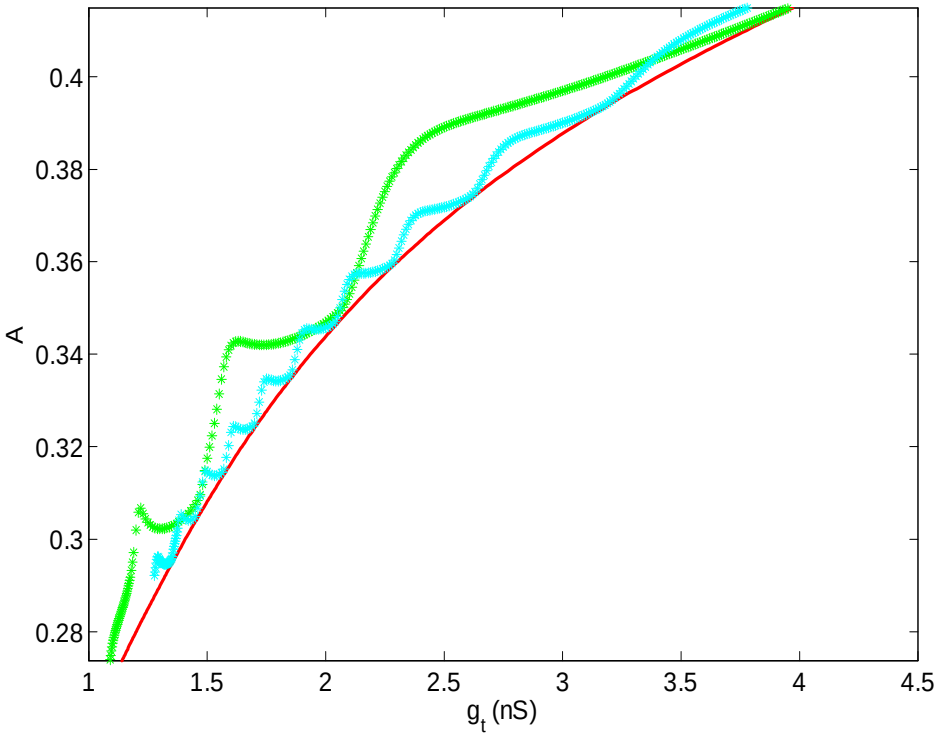

Figure 16. *The stable periodic solution of the detailed system (red line) can be regarded as a stable equilibrium for the simplified system (see insert "B" of Figure 12). Green stars: $\tau = 30$ [ms], cyan stars: $\tau = 120$ [ms]. The EF calculation follows the periodic solution more closely when τ is larger. An explanation for the oscillations is given in the text and in Figure 17.*

4.3. Justification for the subcritical Hopf bifurcation (results in insert "C" of Figure 12). We know that the Hopf bifurcation for the detailed system is also a Hopf bifurcation for the simplified system by looking at the eigenvalues of the simplified system (calculated as described in section 3.3.1) which become unstable by crossing the complex line. The detailed system has a very small region ($0.26045 \leq g_t < 0.2606$) for which the bursting solution coexists with a stable equilibrium (hence a large amplitude periodic solution will coexist with a stable equilibrium in the simplified system), and we know that in the detailed system the Hopf bifurcation is subcritical (see the accompanying supplementary materials file 100457_01.pdf [local/web 56.5KB]). We therefore concluded that the Hopf bifurcation of the simplified system ought to appear subcritical. It should be possible in principle to estimate numerically using our method the second and third derivatives of the simplified system and then use the Hopf bifurcation theory to find out whether a Hopf bifurcation is supercritical or subcritical [16]. We did not attempt to perform such calculations in this example, but it might be worthwhile in other cases where the bifurcation diagram of the detailed system is unavailable.

The results shown in insert "C" of Figure 12 are qualitatively unchanged when $\tau = 120\ ms$ and are not shown here. The only difference is that when $\tau = 120\ ms$ the unstable equilibria

Copyright © by SIAM. Unauthorized reproduction of this article is prohibited.

Downloaded 12/19/19 to 128.112.173.161. Redistribution subject to SIAM license or copyright; see http://www.siam.org/journals/ojsa.php

Downloaded 12/19/19 to 128.112.173.161. Redistribution subject to SIAM license or copyright; see http://www.siam.org/journals/ojsa.php

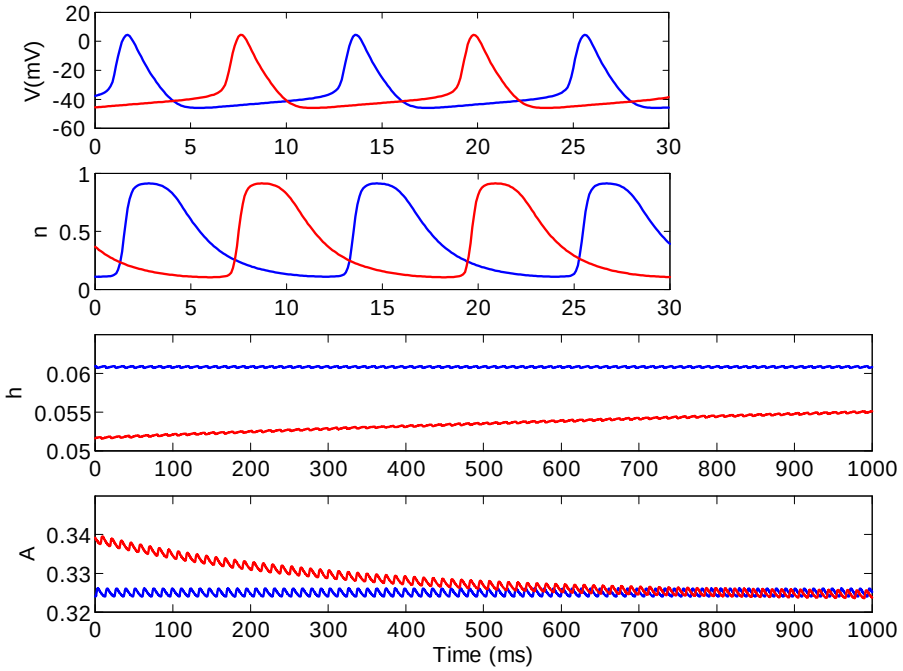

Figure 17. *Comparison of the time evolution of the system following the convergence of the Newton method for the simplified system (red line) with the actual steady state solution (blue line) when $g_t = 1.7$ [nS]. The variables A and h converge slowly to the actual steady state and hence appear like steady state over a short period of time. The small number of action potential over $\tau = 30$ [ms] (upper panel) explains the oscillations seen in Figure 12. $\alpha = 0.003$ [1/ms], $\beta = 0.05$ [1/mv], $\theta = -20$ [mv].*

can be followed up to $g_t = 0.3$ nS (and not up to $g_t = 0.58$ nS, as is the case when $\tau = 30$ ms).

Figure 18 shows a simulation of the detailed system upon convergence of the Newton method for the simplified system (section 3.3.1). The simulation was done during the last lifting near the Hopf bifurcation in insert "C" of Figure 12 ($g_t = 0.26$ nS) when $\tau = 120$ ms. The variables v (the voltage across the neuron membrane) and n (the gating of potassium) converge quickly to a slow manifold that oscillates very slowly (note the slow variation in v; the solution will eventually converge to an equilibrium). This is consistent with small real part of complex eigenvalues for the simplified system near a Hopf bifurcation.

4.4. Justification for the effective saddle-node bifurcation of periodic orbits. In a generic saddle-node bifurcation of periodic orbits, a stable periodic solution merges with an unstable periodic solution at the bifurcation point. Figure 19 shows a projection of the stable solution (solid line, calculated by time simulations) and the unstable solution (dashed line, calculated using AUTO) into the plane (h, A) for three values of α. It can be seen that for $\alpha = 0.003$ and $\alpha = 0.001$ the unstable solution appears below the stable solution but is above the stable solution for $\alpha = 0.0005$. The way the two solutions approach each other in this

Copyright © by SIAM. Unauthorized reproduction of this article is prohibited.

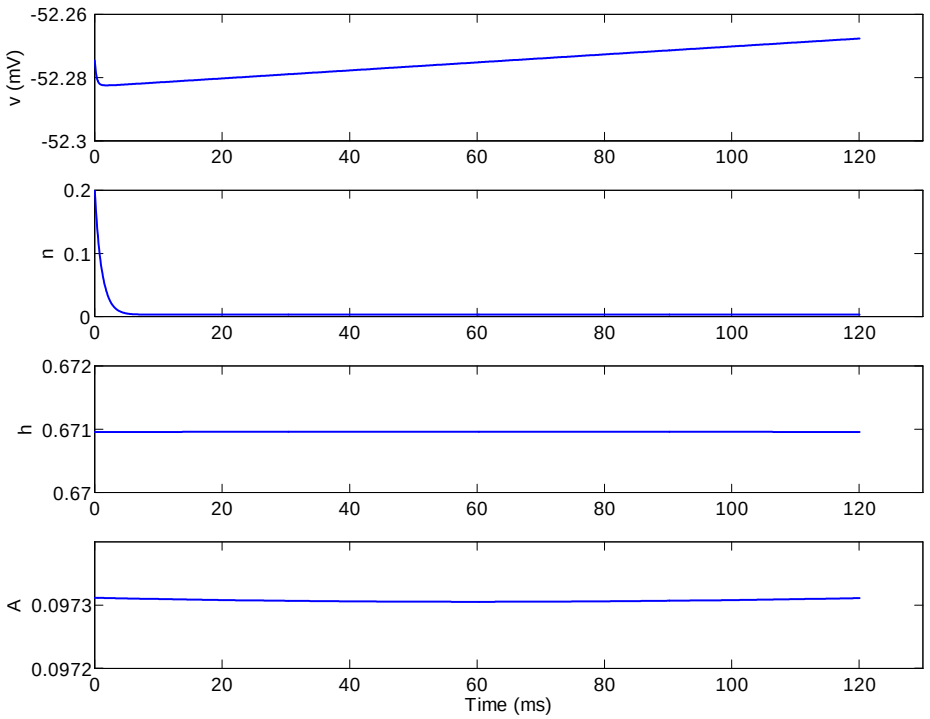

Figure 18. *Simulation of the detailed system during the last lifting upon convergence of the Newton method for the simplified system when $\tau = 120$ [ms] and $g_t = 0.26$ [nS]. v is the voltage across the neuron membrane, n is the gating of potassium, h is the gating of persistent sodium, and A is a measure of the neuron activity. Note the fast convergence of v and n to a slow manifold (which oscillates very slowly) and that the requirement $h(\tau) = h(0)$, $A(\tau) = A(0)$ is met.*

projection suggests that in the simplified system their interaction might appear as a generic saddle-node bifurcation of limit cycles for $0.0005 < \alpha < 0.001$.

5. First steps towards extending the method to a population of neurons. For a population of N neurons we have the following equations:

$$\begin{aligned}
\dot{v}_i &= f_{i1}\left(v_i, n_i, h_i, s_k\right); \quad k = 1, \ldots, N; \quad k \neq i, \\
\dot{n}_i &= f_{i2}\left(v_i, n_i\right), \\
\dot{h}_i &= f_{i3}\left(v_i, h_i\right), \\
\dot{s}_i &= f_{i4}(v_i, s_i), \\
\dot{A} &= \alpha\left(g\left(v\right) - A\right),
\end{aligned}$$

where v_i is the voltage across the membrane of neuron i, n_i is the gating of potassium of neuron i, h_i is the gating of persistent sodium of neuron i, and s_i is a gating variable driven by presynaptic activity which affects the coupling within the population of neurons (note that

Downloaded 12/19/19 to 128.112.173.161. Redistribution subject to SIAM license or copyright; see http://www.siam.org/journals/ojsa.php

Copyright © by SIAM. Unauthorized reproduction of this article is prohibited.

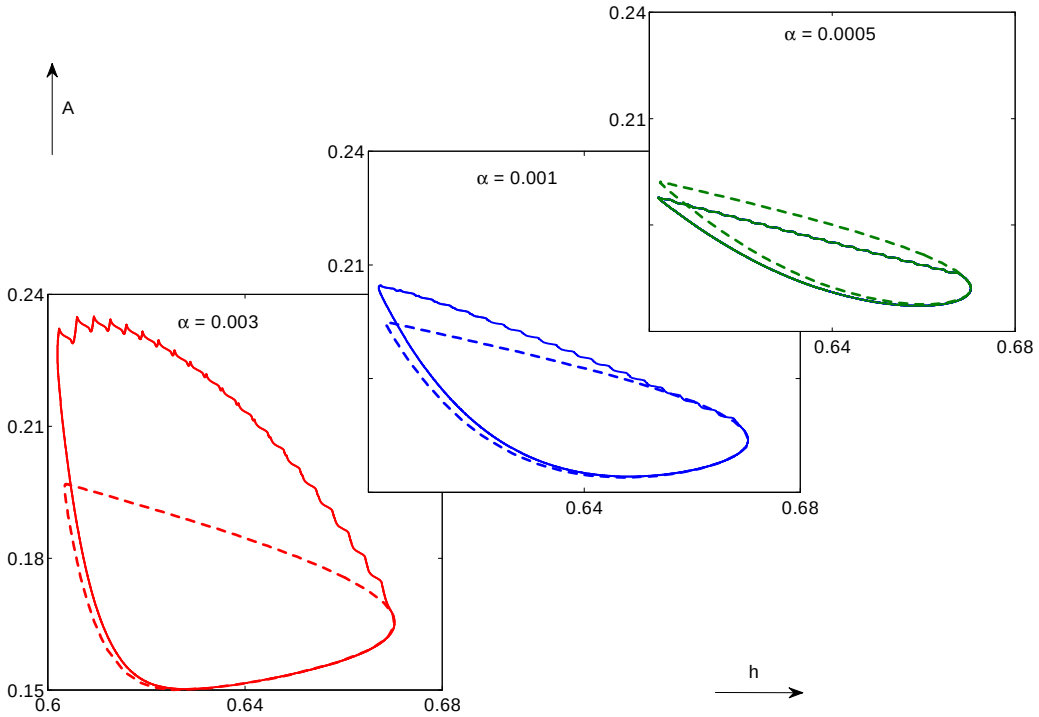

Figure 19. *The projection of a stable solution and an unstable solution of the detailed system may appear as a saddle-node bifurcation of periodic orbits in the simplified system. Each insert shows a stable and an unstable solution at $g_t = 0.2605$ [nS]. The stable solution (solid line) was obtained by time simulation. The unstable solution (dashed line) was generated by AUTO. A generic saddle-node bifurcation is expected to be found for $0.0005 < \alpha < 0.001$ [1/ms]. For all the plots: $\beta = 0.05$ [1/mv], $\theta = -20$ [mv].*

when $N = 1$, $v_1 = f_{11}(v_1, n_1, h_1)$ and the system can be effectively described by (1) and (4)). $g(v)$ is defined as

$$g(v) = \frac{1}{N}\sum_{i=1}^{N} \frac{1}{1 + e^{-\beta(v_i - \theta)}}.$$

The two *global* variables are now A (a single variable for the entire subpopulation) and $\bar{h} = \left(\sum_{i=1}^{i=N} h_i\right)/N$. The restriction and lifting operators are the same as described in section 3.2 except, given $\bar{h}(\tau)$ and $A(\tau)$, we now need to fix $v_i(0)$, $n_i(0)$, and $s_i(0)$, guess $h_i(0)$, and solve (10). If the newly calculated $\tilde{h}(\tau)$ is close enough to the desired (given) value of $\bar{h}(\tau)$, the lifting is complete and the output is $v_i(\tau)$, $n_i(\tau)$, $s_i(\tau)$, and $h_i(\tau)$. If not, we guess new $h_i(0)$ and repeat the process. To guess $h_i(0)$ we first guess $\tilde{h}(0)$ and assign $h_i(0) = \tilde{h}(0)$ (that is, we assume that $h_i(0)$ are the same for all i). The initial guess for $\tilde{h}(0)$ is $\tilde{h}(0) = \bar{h}(\tau)$, and we then improve this guess using the Steffensen method as described in section 3.2.1. We choose values to fix $v_i(0)$ as we did for one neuron but add small noise, $\omega(i)$, to each $v_i(0)$:

$$v_i(0) = -\frac{1}{\beta} ln\left(\frac{1 - A(\tau)}{A(\tau)}\right) + \theta + \omega(i).$$

Copyright © by SIAM. Unauthorized reproduction of this article is prohibited.

Downloaded 12/19/19 to 128.112.173.161. Redistribution subject to SIAM license or copyright; see http://www.siam.org/journals/ojsa.php

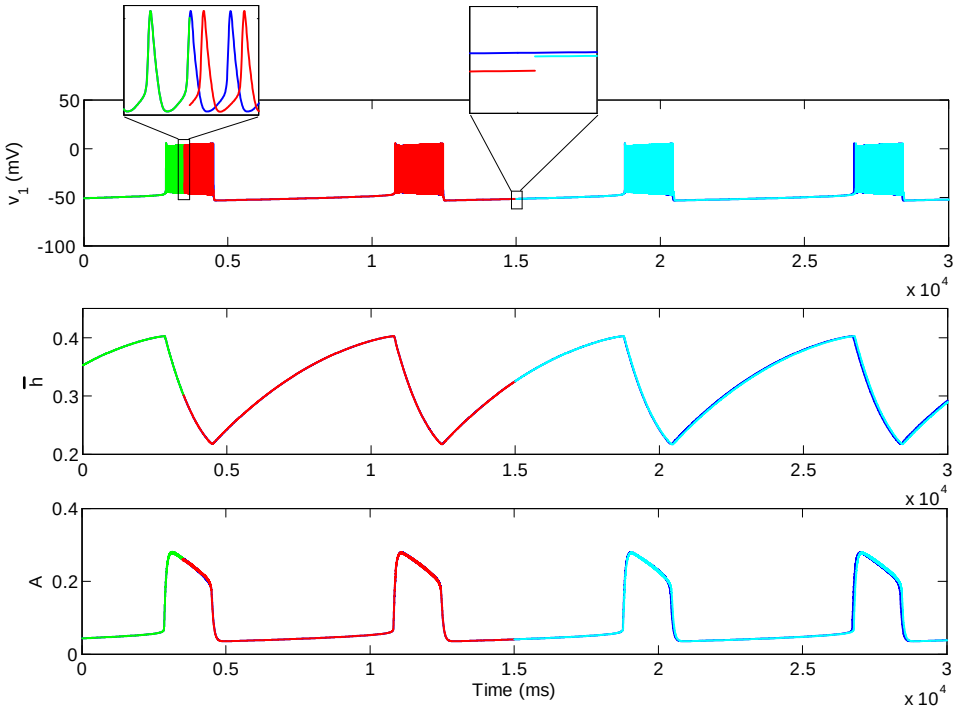

Figure 20. *Examples of successful lifting in a network of* 11 *neurons. The blue line shows an undisturbed simulation. The green line shows the original simulation until it was stopped at* $t = 3.5$ *[s]. The red and cyan lines show the simulation after the lifting operator was used at* $t = 3.5$ *and* $t = 15$ *[s], respectively (the inserts show a closer view near these points).* v_1 *is the voltage across the membrane of one of the* 11 *neurons,* $\bar{h}$ *is the average of gating of persistent sodium, and* A *is a measure of the network activity.* $g_t = 0.5$ *[nS],* $\tau = 120$ *[ms],* $g_{syn}^{i,j} = 0.9$ *[nS] for all* $i \neq j$, $\alpha = 0.015$ *[1/ms],* $\beta = 0.1$ *[1/mv], and* $\theta = -20$ *[mv]; other parameters are given in Appendix* A.

Figure 20 shows examples of successful lifting in a network of 11 neurons (this choice of network is arbitrary and designed to illustrate how the method works for larger networks). The blue line shows an undisturbed simulation. The green line shows the original simulation until it was stopped at $t = 3.5$ s. The red and cyan lines show the simulation after the lifting operator was used at $t = 3.5$ and $t = 15$ s, respectively. All the neurons were identical and connected to all other neurons. Figure 21 shows two examples of successful lifting in the phase plane for the same network. For the 11 neurons network, $\omega(i)$ was a number chosen randomly between 0 and 1 and multiplied by 0.1 and $n_i(0)$ and $s_i(0)$ were chosen as

$$n_i(0) = \frac{1}{1 + e^{-\beta(v_i(0)-\theta)}},$$
$$s_i(0) = \frac{0.2}{1 + e^{-\beta(v_i(0)-\theta)}}.$$

Figure 22 illustrates that our method could be used to generate bifurcation diagrams of coarse network simplifications. We plot the diagram of a two-cell network in Figure 22 because it enables us to compare the coarse diagram with the bifurcation diagram of the detailed sys-

Copyright © by SIAM. Unauthorized reproduction of this article is prohibited.

Downloaded 12/19/19 to 128.112.173.161. Redistribution subject to SIAM license or copyright; see http://www.siam.org/journals/ojsa.php

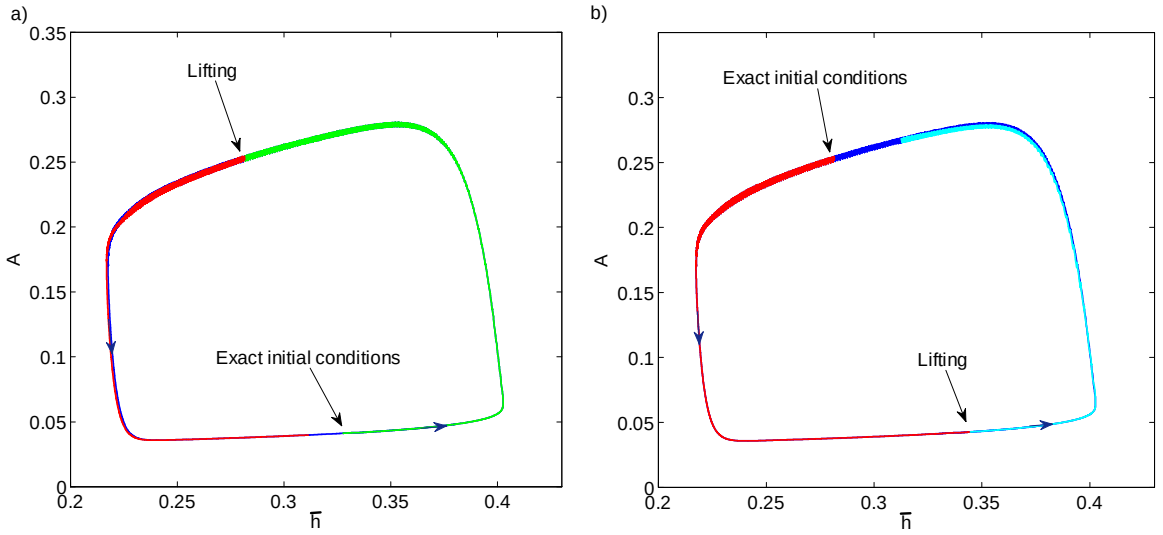

Figure 21. *Examples of successful lifting in the phase plane for a network of* 11 *neurons. In both graphs, the blue line shows an undisturbed simulation and the blue arrows indicate the direction of time.* (a) *The green line shows the original simulation until it was stopped at the active phase, and the red line shows the simulation after the lifting operator was used.* (b) *The red line shows the original simulation until it was stopped at the quiescent phase, and the cyan line shows the simulation after the lifting operator was used. The variables and parameters are the same as in Figure* 20.

tem. The green stars represent stable equilibria and the black circles unstable equilibria, both calculated using the EF approach. Other lines were computed by AUTO using the detailed system (with the exact Jacobian supplied): solid blue lines represent stable equilibria; dot-dashed blue line and dashed black line represent unstable equilibria associated with symmetric and nonsymmetric voltages, respectively; solid red lines represent stable periodic solutions; and dashed red lines represent unstable periodic solutions (in the case of periodic solutions, both the maximum and the minimum are shown). Figure 22 was generated with $\omega(i) = 0$ and with the same choice of $n_i(0)$ and $s_i(0)$ as described above for the 11-neuron system, and $g_{syn}^{i,j}$ was chosen in a region where $h_1 \approx h_2$ (see [5]). Insert "a" shows that two close Hopf bifurcations in the detailed system are regarded as a single Hopf in the coarse system. The early loss of stability might be due to the unstable periodic solution close by. Insert "b" shows that several bifurcation points in the detailed system are ignored in the coarse system. Our method bypasses two Hopf bifurcations and a torus bifurcation of a symmetric periodic solution. Outside insert "b" we also bypass a symmetry breaking bifurcation of the periodic solution. Time traces of v_1 and v_2 are shown for three values of g_t. The program was run until it stopped converging. We could in principle adapt some EF parameters to allow a better trace of the solution as the bifurcation parameter changes, but we did not attempt doing it here.

The choice of $h_i(0) = \tilde{h}(0)$ is not expected to work well when $h_i(t)$ are significantly different. This is because over the short simulation time the slow $h_i(t)$ will not have time to converge. To overcome this problem, the Newton method could be used to calculate each

Copyright © by SIAM. Unauthorized reproduction of this article is prohibited.

Downloaded 12/19/19 to 128.112.173.161. Redistribution subject to SIAM license or copyright; see http://www.siam.org/journals/ojsa.php

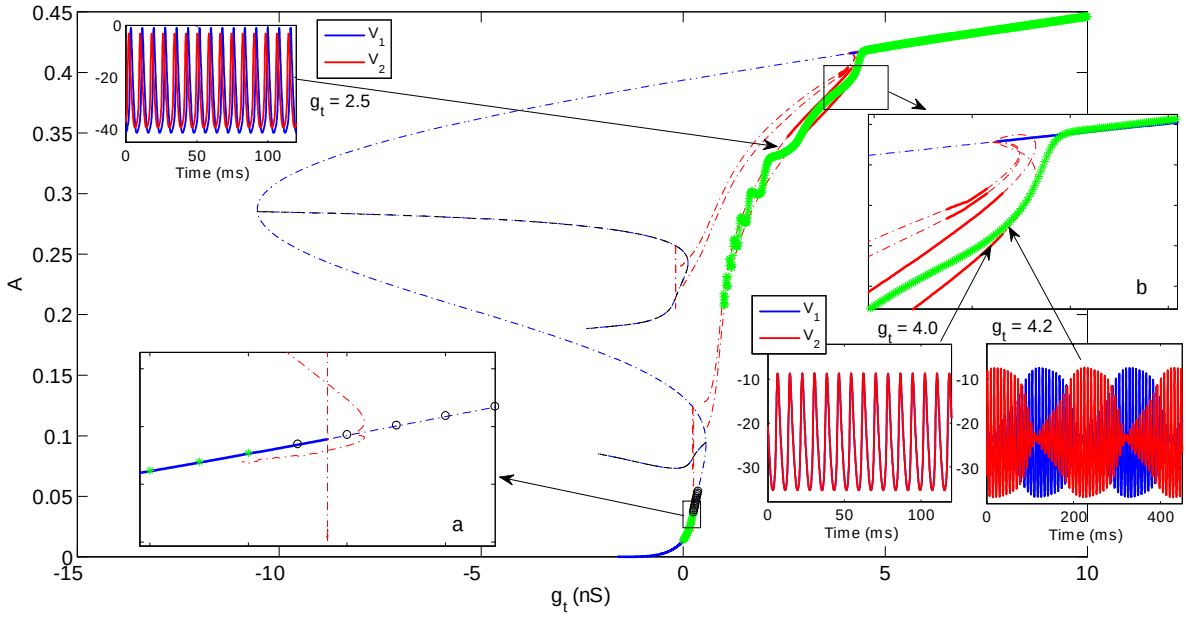

Figure 22. *Using the EF approach to create a partial bifurcation diagram for a network of two cells. Green stars - stable equilibria, black circles - unstable equilibria; both are calculated using the EF approach. Other lines - computed by AUTO using the detailed system; solid blue lines - stable equilibria, dashed-dotted blue lines and dashed black lines - unstable equilibria associated with symmetric and nonsymmetric voltages, respectively, solid red lines - stable periodic, dashed red lines - unstable periodic solutions (the minima and maxima of the solutions are shown).* $g_{syn}^{i,j} = 9$ *[nS] for all* $i \neq j$, $\alpha = 0.015$ *[1/ms],* $\beta = 0.1$ *[1/mv],* $\theta = -20$ *[mv], and* $\tau = 120$ *[ms]; other parameters are given in Appendix* A.

value of $h_i(0)$ separately, but this is left for future investigations.

6. Discussion and conclusions. This paper is motivated by the modelling needs for studying the integrated behavior of the respiratory system at the systems level. It strives to address the following question: Could the dynamics of the pre-BötC (an area of the mammalian brainstem that is essential for the control of breathing) be effectively represented by two ordinary differential equations? More specifically, we asked the following: Could the transitions from the quiescent to bursting to spiking states be represented qualitatively in a way that is consistent with a 2D smooth model? We used an EF approach to perform continuation/bifurcation calculations for a simplified model of a single bursting neuron (that consists of two *unknown* differential equations) and compared it with the bifurcation diagram of the detailed system (that consists of three *known* differential equations of the original system + an additional equation that serves as an observable). The introduction of an "observable" in the present paper represents a unique approach in the EF literature. In its original introduction, the EF method assumed that the coarse-grained variables are available or have been decided upon a priori [41, 15, 18]. It is only in later publications that the issue of establishing good coarse variables arises, and even there the emphasis is more on the use of manifold learning to determine such variables from processing simulation data [10, 36, 13]. Discussions of the type presented in this paper, where an explicit good candidate coarse variable is proposed via the

Copyright © by SIAM. Unauthorized reproduction of this article is prohibited.

Downloaded 12/19/19 to 128.112.173.161. Redistribution subject to SIAM license or copyright; see http://www.siam.org/journals/ojsa.php

Downloaded 12/19/19 to 128.112.173.161. Redistribution subject to SIAM license or copyright; see http://www.siam.org/journals/ojsa.php

introduction of an additional differential equation and then tested/validated, do not arise in the EF literature; there is, however, a case where the nature of the coarse bifurcations expected from the reduced model does arise [27]. This is a discrete problem, which is coarse-grained as a continuous space one, and this drastically changes the wave pinning bifurcations of the fine-scale description. In the context of computational neuroscience, the first use of EF computations is due to Laing [19]. Several additional applications have followed (see, e.g., [21, 20, 23, 28, 22]), but in all of them, again, the coarse variables were either given or obtained through data mining, in contrast to the work in this paper. The use of EF methods in the study of more general networked systems has also been the object of study in recent years (see, for example, [17, 44, 30, 43, 28]), and the subject has been reviewed in [2]. Once again, in these studies the coarse variables are either assumed known or arise from nonlinear manifold-learning algorithms. Although the introduction of an additional differential equation could be thought of as averaging over the fast variable, it differs from the standard averaging methods found in the literature (see, e.g., [5]) in that we do not need to know the period of the periodic solution over which we are averaging, our calculation is done on the full system (not just the fast subsystem), and our method allows for averaging over nonperiodic solutions and moving seemingly between different types of solutions and different parameters.

We argued that for some parameter values a Hopf bifurcation in the original system should be retained by a simplified model while for some other parameter values it could be ignored, and we provided a schematic description of a bifurcation diagram of the simplified system. Although our end result is not a set of equations for the simplified model, it provides a set of properties/features that such a model should include (i.e., the variables and the coarse bifurcation diagram) and hence provides the means to link a phenomenological, ad hoc model more closely to the detailed system. Finding equations that produce the coarse bifurcation diagram is in principle possible since we made sure that the bifurcation diagram is consistent with a 2D smooth model, but this was not done here. We envision that such equations could be developed in the same way phenomenological models have been developed with the additional requirement that they reproduce the coarse bifurcation diagram.

We illustrated our approach on a single neuron. This enabled us to develop and explain the method by separating between the integration over time (which has not been done using the EF approach before) from averaging over the state variables (which is done in addition to the integration over time when we increase the number of neurons). Importantly, studying the single neuron enabled us to validate the method—something that is difficult to do in a large network and indeed has not been done before with the EF approach. The simplification of single neurons provides computational advantages when coupling them in a large network of neurons (see, for example, [31]) or as a representation of a synchronized population of neurons (see, for example, [32]). It is therefore important to understand how good the simplification of a single neuron is and how well its dynamics is represented by the simplified model. Our approach adds another tool to help achieve this goal but does not eliminate completely the need for modelling judgment (i.e., we argue in this paper that the transition from spiking to bursting, represented by a Hopf bifurcation in the simplified system, is not well defined).

Importantly, we have illustrated how our method can be extended to a network of several neurons. Producing bifurcation diagrams of the detailed system is not required in principle but was useful to validate the approach and gain a better understanding of its limitations. It

Copyright © by SIAM. Unauthorized reproduction of this article is prohibited.

is envisioned that further adaptation of the lifting operator will be required when networks with other structures are studied. Exploring what the simplified bifurcation diagram could look like for a specific network, and to what extent the structure of the network affects the properties of a simplified model, also remain for future investigations.

Appendix A. The mathematical equations. We use the model proposed in [8] for a population of N neurons in the pre-BötC:

$$
\begin{aligned}
c\frac{dv_i}{dt} &= -I_{NaP} - I_{Na} - I_K - I_L - I_{syn}^{(i)} - g_t v_i,\\
\frac{dn_i}{dt} &= \alpha_n(1-n_i) - \beta_n n_i,\\
\frac{dh_i}{dt} &= \alpha_h(1-h_i) - \beta_h h_i,\\
\frac{ds_i}{dt} &= \left[\bar{s}(1-s_i) - s_i\right]/\tau_s,
\end{aligned}
\tag{10}
$$

where

$$
\begin{aligned}
I_{NaP} &= g_{NaP}\bar{m}_p h_i (v_i - E_{Na}),\\
I_{Na} &= g_{Na}\bar{m}^3(1-n_i)(v_i - E_{Na}),\\
I_K &= g_k n_i^4 (v_i - E_k),\\
I_L &= g_L(v_i - E_L),\\
I_{syn}^{(i)} &= v_i \sum_{j=1}^{N} g_{syn}^{(i,j)} s_j\,; \quad g_{syn}^{(i,i)} = 0,
\end{aligned}
$$

and

$$
\begin{aligned}
\bar{m}_p &= \left(1 + e^{\frac{v_i - \theta_{mp}}{\sigma_{mp}}}\right)^{-1},\\
\bar{m} &= \left(1 + e^{\frac{v_i - \theta_m}{\sigma_m}}\right)^{-1},\\
\bar{s} &= \left(1 + e^{\frac{v_i - \theta_s}{\sigma_s}}\right)^{-1},\\
\alpha_n &= \frac{1}{2\tau_n} e^{-\frac{v_i - \theta_n}{2\sigma_n}},\\
\beta_n &= \frac{1}{2\tau_n} e^{\frac{v_i - \theta_n}{2\sigma_n}},\\
\alpha_h &= \frac{1}{2\tau_h} e^{-\frac{v_i - \theta_h}{2\sigma_h}},\\
\beta_h &= \frac{1}{2\tau_h} e^{\frac{v_i - \theta_h}{2\sigma_h}},
\end{aligned}
$$

where v_i is the voltage across the membrane of neuron i, n_i is the gating of potassium of neuron i, h_i is the gating of persistent sodium of neuron i, and s_i is a gating variable driven

Copyright © by SIAM. Unauthorized reproduction of this article is prohibited.

Downloaded 12/19/19 to 128.112.173.161. Redistribution subject to SIAM license or copyright; see http://www.siam.org/journals/ojsa.php

Table 1
Parameters used in the simulations.

Symbol	Value	Units	Symbol	Value	Units
C	21.0	pF	θ_{mp}	–40.0	mV
g_{NaP}	2.8	nS	θ_m	–34.0	mV
g_{Na}	28.0	nS	θ_n	–29.0	mV
g_k	11.2	nS	θ_h	–48.0	mV
g_L	2.8	nS	θ_s	–10.0	mV
E_{Na}	50.0	mV	σ_{mp}	–6.0	mV
E_k	–85.0	mV	σ_m	–5.0	mV
E_L	–65.0	mV	σ_n	–4.0	mV
τ_h	10.0	s	σ_h	6.0	mV
τ_n	10.0	ms	σ_s	–5.0	mV
τ_s	5.0	ms			

by presynaptic activity which affects the coupling within the population of neurons. Note that when $N = 1$ (a single neuron), $I_{syn}^{(1)} = 0$ and the neuron dynamics can be described effectively by three ordinary differential equations for v_1, n_1, and h_1.

The parameters we use in the simulations are given in Table 1 (the parameters g_t and $g_{syn}^{(i,j)}$ are given in the text).

Note that the parameters we use here are the same as in [5] and differ slightly from those used in [7] (the value of E_L is $-60.0\ mV$ in [7]).

Acknowledgments. We would like to acknowledge Joshua Duley, who contributed to this project as a summer student in 2012. We are grateful for the useful suggestions we received from the anonymous referees. We would also like to thank Vivien Kirk for reading and commenting on the first version of this paper.

REFERENCES

[1] R. Barrio, M. A. Martinez, S. Serrano, and A. Shilnikov, *Macro- and micro-chaotic structures in the Hindmarsh-Rose model of bursting neurons*, Chaos, 24 (2014), 023128, doi:10.1063/1.4882171.

[2] K. A. Bold, K. Rajendran, B. Ráth, and I. G. Kevrekidis, *An equation-free approach to coarse-graining the dynamics of networks*, J. Comput. Dyn., 1 (2014), pp. 111–134, doi:10.3934/jcd.2014.1.111.

[3] A. Ben-Tal and J. C. Smith, *A model for control of breathing in mammals: Coupling neural dynamics to peripheral gas exchange and transport*, J. Theoret. Biol., 251 (2008), pp. 480–497, doi:10.1016/j.jtbi.2007.12.018.

[4] A. Ben-Tal and J. C. Smith, *Control of breathing: Two types of delays studied in an integrated model of the respiratory system*, Respir. Physiol. Neurobiol., 170 (2010), pp. 103–112, doi:10.1016/j.resp.2009.10.008.

[5] J. Best, A. Borisyuk, J. Rubin, D. Terman, and M. Wechselberger, *The dynamic range of bursting in a model respiratory pacemaker network*, SIAM J. Appl. Dyn. Syst., 4 (2005), pp. 1107–1139, doi:10.1137/050625540.

[6] S. Boie, V. Kirk, J. Sneyd, and M. Wechselberger, *Effects of quasi-steady-state reduction on biophysical models with oscillations*, J. Theoret. Biol., 393 (2016), pp. 16–31, doi:10.1016/j.jtbi.2015.12.011.

[7] R. J. Butera, J. Rinzel, and J. C. Smith, *Models of respiratory rhythm generation in the pre-Bötzinger complex.* I. *Bursting pacemaker neurons*, J. Neurophysiol., 81 (1999), pp. 382–397.

Copyright © by SIAM. Unauthorized reproduction of this article is prohibited.

Downloaded 12/19/19 to 128.112.173.161. Redistribution subject to SIAM license or copyright; see http://www.siam.org/journals/ojsa.php

[8] R. J. Butera, J. Rinzel, and J. C. Smith, *Models of respiratory rhythm generation in the pre-Bötzinger complex.* II. *Populations of coupled pacemaker neurons*, J. Neurophysiol., 81 (1999), pp. 398–415.
[9] N. S. Cherniack, G. Longobardo, and C. J. Evangelista, *Causes of Cheyne-Stokes respiration*, Neurocrit. Care, 3 (2005), pp. 271–279, doi:10.1385/ncc:3:3:271.
[10] R. Erban, T. A. Frewen, X. Wang, T. C. Elston, R. Coifman, B. Nadler, and I. G. Kevrekidis, *Variable-free exploration of stochastic models: A gene regulatory network example*, J. Chem. Phys., 126 (2007), 155103, doi:10.1063/1.2718529.
[11] B. Ermentrout and D. H. Terman, *Mathematical Foundations of Neuroscience*, Springer, New York, 2010.
[12] J. L. Feldman, C. A. Del Negro, and P. A. Gray, *Understanding the rhythm of breathing: So near, yet so far*, Annu. Rev. Physiol., 75 (2013), pp. 423–452, doi:10.1146/annurev-physiol-040510-130049.
[13] A. L. Ferguson, A. Z. Panagiotopoulos, I. G. Kevrekidis, and P. G. Debenedetti, *Nonlinear dimensionality reduction in molecular simulation: The diffusion map approach*, Chem. Phys. Lett., 509 (2011), pp. 1–11, doi:10.1016/j.cplett.2011.04.066.
[14] C. Gaiteri and J. E. Rubin, *The interaction of intrinsic dynamics and network topology in determining network burst synchrony*, Front. Comput. Neurosci., 5 (2011), pp. 1–14, doi:10.3389/fncom.2011.00010
[15] C. W. Gear, I. G. Kevrekidis, and C. Theodoropoulos, *"Coarse" integration/bifurcation analysis via microscopic simulators: Micro-Galerkin methods*, Comput. Chem. Eng., 26 (2002), pp. 941–963, doi:10.1016/s0098-1354(02)00020-0.
[16] P. Glendinning, *Stability, Instability and Chaos: An Introduction to the Theory of Nonlinear Differential Equations*, Cambridge University Press, Cambridge, UK, 1994.
[17] T. Gross and I. G. Kevrekidis, *Robust oscillations in SIS epidemics on adaptive networks: Coarse graining by automated moment closure*, Europhys. Lett. EPL, 82 (2008), 38004, doi:10.1209/0295-5075/82/38004.
[18] I. Kevrekidis, C. W. Gear, J. M. Hyman, P. G. Kevrekidis, O. Runborg, and C. Theodoropoulos, *Equation-free, coarse-grained multiscale computation: Enabling microscopic simulators to perform system-level analysis*, Commun. Math. Sci., 1 (2003), pp. 715–762, http://projecteuclid.org/euclid.cms/1119655353.
[19] C. R. Laing, *On the application of "equation-free modelling" to neural systems*, J. Comput. Neurosci., 20 (2006), pp. 5–23, doi:10.1007/s10827-006-3843-z.
[20] C. R. Laing, T. Frewen, and I. G. Kevrekidis, *Reduced models for binocular rivalry*, J. Comput. Neurosci., 28 (2010), pp. 459–476, doi:10.1007/s10827-010-0227-6.
[21] C. R. Laing, T. A. Frewen, and I. G. Kevrekidis, *Coarse-grained dynamics of an activity bump in a neural field model*, Nonlinearity, 20 (2007), pp. 2127–2146, doi:10.1088/0951-7715/20/9/007.
[22] C. R. Laing and I. G. Kevrekidis, *Equation-free analysis of spike timing dependent plasticity*, Biol. Cybernet., 109 (2015), pp. 701–714, doi:10.1007/s00422-015-0668-0.
[23] C. R. Laing, Y. Zou, B. Smith, and I. G. Kevrekidis, *Managing heterogeneity in the study of neural oscillator dynamics*, J. Math. Neurosci., 2 (2012), 5, doi:10.1186/2190-8567-2-5.
[24] B. G. Lindsey, I. A. Rybak, and J. C. Smith, *Computational models and emergent properties of respiratory neural networks*, Compr. Physiol., 2 (2012), pp. 1619–1670, doi:10.1002/cphy.c110016.
[25] E. Manica, G. S. Medvedev, and J. E. Rubin, *First return maps for the dynamics of synaptically coupled conditional bursters*, Biol. Cybernet., 103 (2010), pp. 87–104, doi:10.1007/s00422-010-0399-1.
[26] C. Marschler, J. Sieber, R. Berkemer, A. Kawamoto, and J. Starke, *Implicit methods for equation-free analysis: Convergence results and analysis of emergent waves in microscopic traffic models*, SIAM J. Appl. Dyn. Syst., 13 (2014), pp. 1202–1238, doi:10.1137/130913961.
[27] J. Moller, O. Runborg, P. G. Kevrekidis, K. Lust, and I. G. Kevrekidis, *Equation-free, effective computation for discrete systems: A time stepper based approach*, Internat. J. Bifur. Chaos Appl. Sci. Engrg., 15 (2005), pp. 975–996, doi:10.1142/s0218127405012399.
[28] S. J. Moon, K. A. Cook, K. Rajendran, I. G. Kevrekidis, J. Cisternas, and C. R. Laing, *Coarse-grained clustering dynamics of heterogeneously coupled neurons*, J. Math. Neurosci., 5 (2015), 2, doi:10.1186/2190-8567-5-2.
[29] M. T. Naughton, *Cheyne-Stokes respiration: Friend or foe?*, Thorax, 67 (2012), pp. 357–360, doi:10.1136/thoraxjnl-2011-200927.

Downloaded 12/19/19 to 128.112.173.161. Redistribution subject to SIAM license or copyright; see http://www.siam.org/journals/ojsa.php

Copyright © by SIAM. Unauthorized reproduction of this article is prohibited.

[30] K. Rajendran and I. G. Kevrekidis, *Coarse graining the dynamics of heterogeneous oscillators in networks with spectral gaps*, Phys. Rev. E (3), 84 (2011), 036708, doi:10.1103/PhysRevE.84.036708.
[31] J. Rubin and D. Terman, *Synchronized activity and loss of synchrony among heterogeneous conditional oscillators*, SIAM J. Appl. Dyn. Syst., 1 (2002), pp. 146–174, doi:10.1137/S111111110240323X.
[32] J. E. Rubin, N. A. Shevtsova, G. B. Ermentrout, J. C. Smith, and I. A. Rybak, *Multiple rhythmic states in a model of the respiratory central pattern generator*, J. Neurophysiol., 101 (2009), pp. 2146–2165, doi:10.1152/jn.90958.2008.
[33] L. R. Scott, *Numerical Analysis*, Princeton University Press, Princeton, NJ, 2011.
[34] A. Shilnikov, *Complete dynamical analysis of a neuron model*, Nonlinear Dynam., 68 (2012), pp. 305–328, doi:10.1007/s11071-011-0046-y.
[35] A. Shilnikov, R. L. Calabrese, and G. Cymbalyuk, *Mechanism of bistability: Tonic spiking and bursting in a neuron model*, Phys. Rev. E (3), 71 (2005), 056214, doi:10.1103/PhysRevE.71.056214.
[36] A. Singer, R. Erban, I. G. Kevrekidis, and R. R. Coifman, *Detecting intrinsic slow variables in stochastic dynamical systems by anisotropic diffusion maps*, Proc. Natl. Acad. Sci. USA, 106 (2009), pp. 16090–16095, doi:10.1073/pnas.0905547106.
[37] J. C. Smith, A. P. L. Abdala, I. A. Rybak, and J. F. R. Paton, *Structural and functional architecture of respiratory networks in mammalian brainstem*, Philos. Trans. R. Soc. Lond. B Biol. Sci., 364 (2009), pp. 2577–2587, doi:10.1098/rstb.2009.0081.
[38] J. C. Smith, H. H. Ellenberger, K. Ballanyi, D. W. Richter, and J. L. Feldman, *Pre-Bötzinger complex: A brainstem region that may generate respiratory rhythm in mammals*, Science, 254 (1991), pp. 726–729.
[39] D. Terman, *Chaotic spikes arising from a model of bursting in excitable membranes*, SIAM J. Appl. Math., 51 (1991), pp. 1418–1450, doi:10.1137/0151071.
[40] D. Terman, *The transition from bursting to continuous spiking in excitable membrane models*, J. Nonlinear Sci., 2 (1992), pp. 135–182.
[41] C. Theodoropoulos, Y. H. Qian, and I. G. Kevrekidis, *"Coarse" stability and bifurcation analysis using time-steppers: A reaction-diffusion example*, Proc. Natl. Acad. Sci. USA, 97 (2000), pp. 9840–9843, doi:10.1073/pnas.97.18.9840.
[42] N. Toporikova and R. J. Butera, *Dynamics of neuromodulatory feedback determines frequency modulation in a reduced respiratory network: A computational study*, Respir. Physiol. Neurobiol., 185 (2013), pp. 582–592, doi:10.1016/j.resp.2012.11.013.
[43] A. C. Tsoumanis, K. Rajendran, C. I. Siettos, and I. G. Kevrekidis, *Coarse-graining the dynamics of network evolution: The rise and fall of a networked society*, New J. Phys., 14 (2012), 083037, doi:10.1088/1367-2630/14/8/083037.
[44] A. C. Tsoumanis, C. I. Siettos, G. V. Bafas, and I. G. Kevrekidis, *Equation-free multiscale computations in social networks: From agent-based modeling to coarse-grained stability and bifurcation analysis*, Internat. J. Bifur. Chaos Appl. Sci. Engrg., 20 (2010), pp. 3673–3688, doi:10.1142/s0218127410027945.
[45] C. Vandekerckhove, B. Sonday, A. Makeev, D. Roose, and I. G. Kevrekidis, *A common approach to the computation of coarse-scale steady states and to consistent initialization on a slow manifold*, Comput. Chem. Eng., 35 (2011), pp. 1949–1958, doi:10.1016/j.compchemeng.2010.12.002.

Downloaded 12/19/19 to 128.112.173.161. Redistribution subject to SIAM license or copyright; see http://www.siam.org/journals/ojsa.php

Copyright © by SIAM. Unauthorized reproduction of this article is prohibited.